Combining X-ray Crystallography and Molecular Modeling toward the Optimization of Pyrazolo[3,4-*d*]pyrimidines as Potent c-Src Inhibitors Active in Vivo against Neuroblastoma

Cristina Tintori,[†] Anna Lucia Fallacara,[†,‡] Marco Radi,[†,◆] Claudio Zamperini,[†] Elena Dreassi,[†] Emmanuele Crespan,[§] Giovanni Maga,[§] Silvia Schenone,*[‖] Francesca Musumeci,[‖] Chiara Brullo,[‖] André Richters,[⊥] Francesca Gasparrini,[#] Adriano Angelucci,[∇] Claudio Festuccia,[∇] Simona Delle Monache,[∇] Daniel Rauh,[⊥] and Maurizio Botta[†,○]

[†]Dipartimento di Biotecnologie, Chimica e Farmacia, Università degli Studi di Siena Via Aldo Moro 2, 53100 Siena, Italy

[‡]Dipartimento di Chimica e Tecnologie Farmaceutiche, Sapienza Università di Roma, Piazzale Aldo Moro 5, 00185 Roma, Italy

[§]Istituto di Genetica Molecolare, IGM-CNR, Via Abbiategrasso 207, 27100 Pavia, Italy

[‖]Dipartimento di Farmacia, Università degli Studi di Genova, Viale Benedetto XV, 3, 16132 Genova, Italy

[⊥]Department of Chemistry and Chemical Biology, Technical University of Dortmund, Otto-Hahn-Strasse 6, 44227 Dortmund, Germany

[#]Dipartimento di Medicina Molecolare, Sapienza Università di Roma, Piazzale Aldo Moro 5, 00185 Roma, Italy

[∇]Dipartimento di Scienze Cliniche Applicate e Biotecnologiche, Università degli Studi dell'Aquila, Via Vetoio, 67100 Coppito, L'Aquila, Italy

[○]Sbarro Institute for Cancer Research and Molecular Medicine, Center for Biotechnology, College of Science and Technology, Temple University, BioLife Science Building, Suite 333, 1900 North 12th Street, Philadelphia, Pennsylvania 19122, United States

S *Supporting Information*

ABSTRACT: c-Src is a tyrosine kinase belonging to the Src-family kinases. It is overexpressed and/or hyperactivated in a variety of cancer cells, thus its inhibition has been predicted to have therapeutic effects in solid tumors. Recently, the pyrazolo[3,4-*d*]pyrimidine **3** was reported as a dual c-Src/Abl inhibitor. Herein we describe a multidisciplinary drug discovery approach for the optimization of the lead **3** against c-Src. Starting from the X-ray crystal structure of c-Src in complex with **3**, Monte Carlo free energy perturbation calculations were applied to guide the design of c-Src inhibitors with improved activities. As a result, the introduction of a *meta* hydroxyl group on the C4 anilino ring was computed to be particularly favorable. The potency of the synthesized inhibitors was increased with respect to the starting lead **3**. The best identified compounds were also found active in the inhibition of neuroblastoma cell proliferation. Furthermore, compound **29** also showed in vivo activity in xenograft model using SH-SY5Y cells.
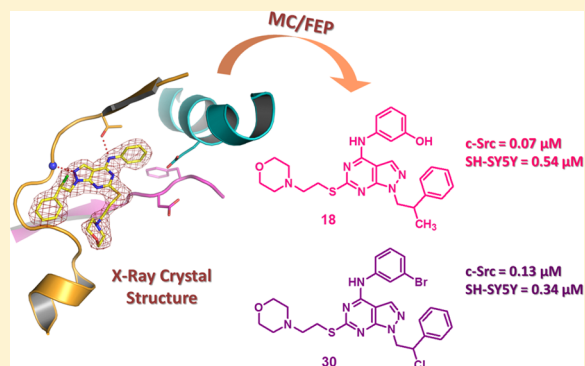
INTRODUCTION

Neuroblastoma (NB) is a rare cancer of the sympathetic nervous system. It accounts for about 9% of malignancies in patients younger than 15 years and for around 15% of all pediatric oncology deaths.[1] It is the most common extracranial solid tumor in childhood and is a major cause of death from neoplasia in infancy.[2] The disease is remarkable for its broad spectrum of clinical behavior. Although during the past few decades a substantial improvement in the treatment of certain, well-defined, subsets of patients has been observed, the outcome of the disease for children with a high-risk clinical phenotype has improved modestly, with long-term survival less than 40%.[3,4] The therapeutic options for the clinical managing of NB consist of a multimodality approach, which includes surgery, chemotherapy, radiotherapy, and biotherapy. Current chemotherapeutic treatment for high-risk neuroblastoma uses dose-intensive cycles of cisplatin and etoposide, alternating with vincristine, doxorubicin, and cyclophosphamide. Furthermore, isotretinoin could be used during the first remission. Despite improvements in the overall cure rate of these patients, the treatment strategies are still far from satisfaction especially

because of the severe side effects.[5,6] Accordingly, novel therapeutic approaches are needed to improve the prognosis of patients with NB. Since deregulation of tyrosine kinases (TKs) has been associated with cancer, small molecule TK inhibitors (TKIs) represent one of the largest drug family currently targeted by pharmaceutical companies and academia for the treatment of malignancies. Remarkably, TKIs, acting on specific molecular targets, could be related with reduced toxic side effects during antitumor treatments. For this reason, many TKIs have been tested for their in vitro antiproliferative activity and in vivo anticancer activity, and some of them have been approved in clinical trials or are currently utilized in cancer therapy.[7,8] A subclass of nonreceptor TKs as target in the treatment of human cancers is the Src-family tyrosine kinases (SFKs). Among these, c-Src was found to stimulate cell proliferation, migration, and invasion as well as angiogenesis.[9] Hyperactivation of c-Src causes aberrant cell activity that contributes to cancer development. High expression levels of c-Src have been detected in several cancers and are generally correlated to a poor prognosis with respect to overall survival. Moreover, recent studies suggest that c-Src could be associated with the development of acquired drug resistance.[10] Accordingly, many small molecule c-Src inhibitors have been developed in the last 20 years belonging to different chemical families such as purines,[11,12] anilinoquinazolines,[13] quinoline-carbonitriles,[14] benzotriazines,[15] and thiazole-carboxamides.[16] Remarkably, Src inhibitors showed antitumor effects in multiple solid tumor types.[17] Furthermore, it has been recently reported that, among TKs, c-Src also plays a key role in the differentiation, cell adhesion, and survival of NB cells, due to its hyperactivation rather than overexpression.[18] c-Src was also hypothesized to have an oncogenic role in the progression of aggressive NB forms.[19] Addressing this kinase with small molecule inhibitors and thereby inhibiting its catalytic activity has recently been reported as an effective approach to the treatment of NB. As a proof of concept, the well-known c-Src inhibitor PP2 has recently been proved to inhibit cell survival/proliferation and to reduce aggregation in NB cell lines[20] while the dual Src/Abl inhibitor Dasatinib has been proved to be effective in reducing NB growth both in vitro and in vivo (Figure 1).[21] In recent years, our group conducted extensive studies on a series of novel c-Src/Abl inhibitors endowed with a pyrazolo[3,4-*d*]pyrimidine scaffold.[22] Several members of this family were found to induce apoptosis and to reduce cell proliferation in different solid tumor cell lines (A431, 8701-BC, SaOS-2, and PC3). A selected member of this family (compound 1, Figure 1), characterized by a C6 methylthio group on the pyrazolo[3,4-*d*]pyrimidine scaffold, displayed a promising antiproliferative activity in SH-SY5Y cell cultures of human neuroblastoma.[23] Compound 1 has also been tested on a panel of TKs showing an appreciable selectivity for Src.[24]

To get further insight into the potentiality of such pyrazolo[3,4-*d*]pyrimidines for the treatment of NB, a small collection of closely related analogues characterized by the presence of a C6 methylthio group was synthesized to explore the role of different functional groups in N1 and C4 for the biological activity. Among the synthesized analogues, compound 2 (Figure 1) was characterized by a potent inhibitory activity against c-Src (K_i = 90 nM) and a considerable antiproliferative effect on SH-SY5Y cells (IC$_{50}$ = 80 nM). However, despite its remarkable activities, this compound suffers from a low water solubility (0.12 μg/mL) which precludes oral administration.[25] Accordingly, a series of more
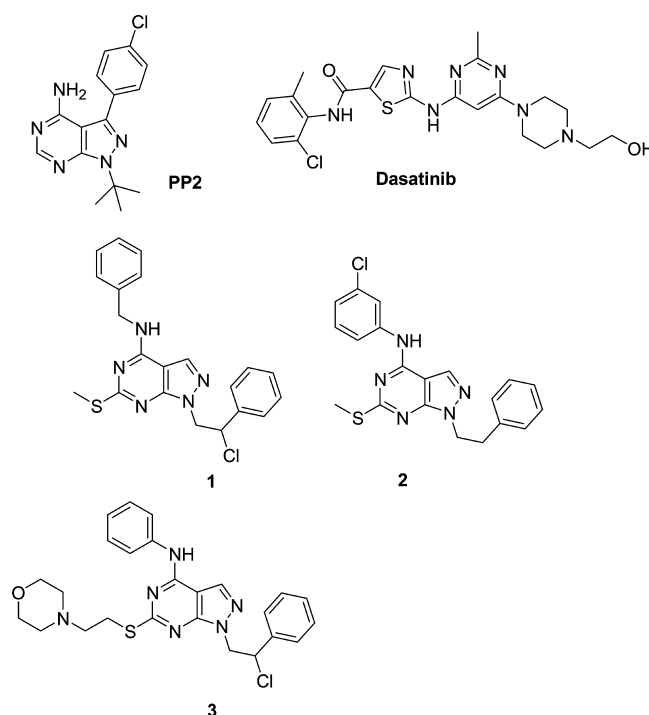

Figure 1. Molecular structure of **PP2**, Dasatinib, and compounds **1**, **2**, and **3**.

soluble pyrazolo[3,4-*d*]pyrimidine derivatives has been rationally designed and synthesized by our research group through the introduction of polar groups in the solvent-exposed C6 position. This study led to the identification of the C4-anilino derivative **3** (Figure 1), which showed a beneficial profile in term of both biological activity and ADME properties, being characterized by a high metabolic stability (95%), a good water solubility (1.7 μg/mL), an efficient membrane permeability (10 × 10^{-6} cm/s), and a potent inhibitory activity against isolated c-Src (K_i = 0.21 μM).[19] Herein, taking into account these preliminary data, we focus our effort on compound **3** with the aim of developing second-generation inhibitors endowed with improved affinity values toward c-Src and improved ADME properties to be tested against neuroblastoma in vivo. To this aim, a multidisciplinary approach combining X-ray crystallography, structure-based drug design, synthesis, in vitro ADME profiling, and in vitro/in vivo biological evaluation was applied. Starting from the crystallographic complex of **3** and c-Src, an efficient optimization of the pyrazolo[3,4-*d*]pyrimidine substituents has been guided by free energy perturbation (FEP) calculations to direct the synthesis of c-Src inhibitors **5−29** (Table 1), many of which are endowed with nanomolar potencies. A subset of compounds also showed a strong antiproliferative activity against SHSY-5Y neuroblastoma cells as well as optimal ADME characteristics. Accordingly, further studies were conducted on compound **29**, which is one of the most promising derivatives, in order to test its efficacy against neuroblastoma in vivo after oral administration in mice.

■ RESULTS AND DISCUSSION

X-ray Structure and Computational Studies. To gain a deeper structural understanding of C6 substituted derivatives binding mode, we determined the crystal structure of a complex of the kinase domain of c-Src (aa 256−533) and the hit compound **3** (see Experimental Section for detailed informa-

Table 1. Enzymatic Activity, Cellular Activity, and ADME Properties of Compounds 3−29

Cpd	R	R¹	R²	c-Src K_i (μM)[a]	Abl K_i (μM)[a]	SH-SY5Y (Spheroid) IC_{50} (μM)	Solubility (μg/mL)	PAMPA P_{app} 10^{-6} cm/sec	Met. Stab. human (%)[b]
					Biological Data			In vitro ADME	
3*	Cl	CH_2CH_2-4-morpholino	$-C_6H_5$	0.24	0.22		1.7	10.0	95
3-R	Cl	CH_2CH_2-4-morpholino	$-C_6H_5$	0.20					
3-S	Cl	CH_2CH_2-4-morpholino	$-C_6H_5$	0.23					
4*	Cl	CH_2CH_2-4-morpholino	$-C_6H_4$-mCl	0.29	0.18		0.1	9.5	95
5*	H	CH_3	$-C_6H_5$	1.46				7.60	90
6	H	CH_3	$-C_6H_4$-mF	1.06				9.33	
7	H	CH_3	$-C_6H_4$-mBr	0.20				3.26	
8*	H	CH_3	$-C_6H_4$-mOH	0.62				5.24	
9	H	CH_2CH_2-4-morpholino	$-C_6H_4$-mCl	1.20				3.50	
10	H	CH_2CH_2-4-morpholino	$-C_6H_4$-mOH ·HCl	0.04	0.13	0.9	97	6.38	97
11	CH_3	CH_2CH_3	$-C_6H_4$-mF	0.79				1.72	94
12	CH_3	CH_2CH_3	$-C_6H_4$-mCl	0.55				3.81	
13	CH_3	CH_2CH_3	$-C_6H_4$-mBr	0.10				2.03	
14	CH_3	CH_2CH_3	$-C_6H_4$-mOH	0.11				4.91	
15	CH_3	CH_2CH_2-4-morpholino	$-C_6H_5$	1.44				3.66	
16	CH_3	CH_2CH_2-4-morpholino	$-C_6H_4$-mF	2.34				6.51	
17	CH_3	CH_2CH_2-4-morpholino	$-C_6H_4$-mCl	0.97				5.51	
18	CH_3	CH_2CH_2-4-morpholino	$-C_6H_4$-mOH ·HCl	0.07	0.43	0.54	1	6.81	99
19	Cl	CH_3	$-C_6H_4$-mOH	0.03	0.15	0.12	4.3	5.92	98
20	Cl	$CH_2CH_2CH_2CH_3$	$-C_6H_4$-mOH	0.13				3.43	
21	Cl	$CH(CH_3)_2$	$-C_6H_5$	0.3					
22	Cl	$CH(CH_3)_2$	$-C_6H_4$-mF	0.26					
23	Cl	$CH(CH_3)_2$	$-C_6H_4$-mBr	0.62					
24	Cl	$CH(CH_3)_2$	$-C_6H_4$-mOH	0.01	0.12	1.53	0.9	4.53	95
25	Cl	cyclopentyl	$-C_6H_5$	0.12				13	94
26	Cl	cyclopentyl	$-C_6H_4$-mF	0.11				14	95
27*	Cl	cyclopentyl	$-C_6H_4$-mCl	NA					
28	Cl	cyclopentyl	$-C_6H_4$-mOH	0.007	0.15	0.62	0.6	3.91	91
29	Cl	CH_2CH_2-4-morpholino	$-C_6H_4$-mBr	0.13	0.12	0.34	3.7	5.27	96

[a]Values are the mean of at least two experiments. [b]Expressed as percentage of unmodified parent drug. *Compounds previously published,[26,33,34] which have been retested according with the conditions described in Experimental Section. Empty cell means not determined.

tion and statistics). Diffraction data was collected to 2.1 Å resolution, and subsequent data processing and refinement exhibited two protein molecules within the crystallographic cell unit which in this work will be referred to as chain A and chain B. Comparative analysis of the empirically determined protein−ligand structure and previous docking studies illustrated coincident binding modes of 3 with respect to c-Src (Figure 2A).[25] The C4 anilino substituent and the N1 side chain are located within the hydrophobic regions I and II, respectively. Furthermore, the X-ray structure confirmed the presence of two predicted hydrogen bonds, involving the C4 amino group which interacts with Thr338 side chain and the N2 of the pyrazolopyrimidine scaffold taking contacts with the backbone of Met341. Remarkably, the same binding orientation was observed for compound 3 within the ATP binding pocket of each chain (Figure 2B). However, despite many residues of the activation loop were poorly defined (from 413 to 424 in chain A and from 411 to 424 in chain B) significant differences between the two chains were observed in the 3D rearrangement of such flexible loop (aa 402−423) as well as in the position of
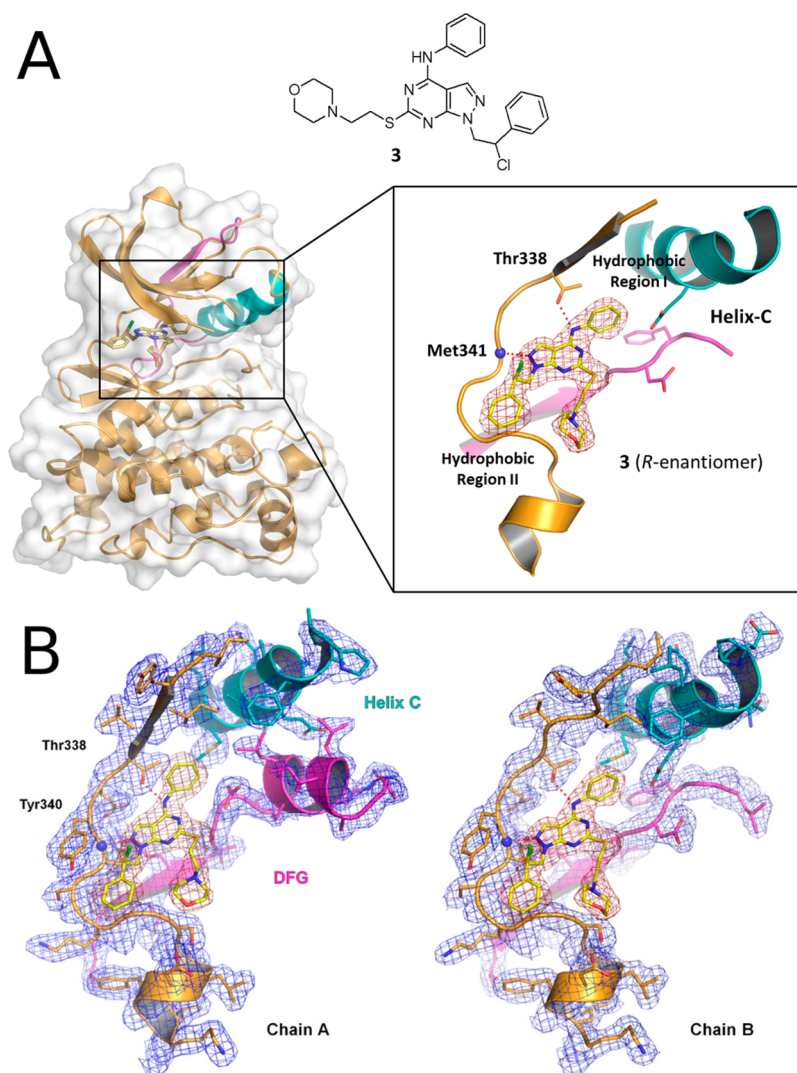
Figure 2. (A) Inhibitor **3** in complex with wild-type c-Src (PDB code: 4O2P). The experimental electron density of **3** at 2.1 Å resolution is displayed ($2F_o - F_c$ map contoured at 1σ). The kinase domain is in the active DFG-in conformation and hydrogen-bond interactions of the inhibitor with Thr338 (gatekeeper) and the backbone amide of Met341 are illustrated as red dotted lines. Hinge region (orange), helix C (turquoise), DFG-motif (pink) and inhibitor **3** (yellow sticks). (B) Experimental electron density of chain A and B in complex with **3**.
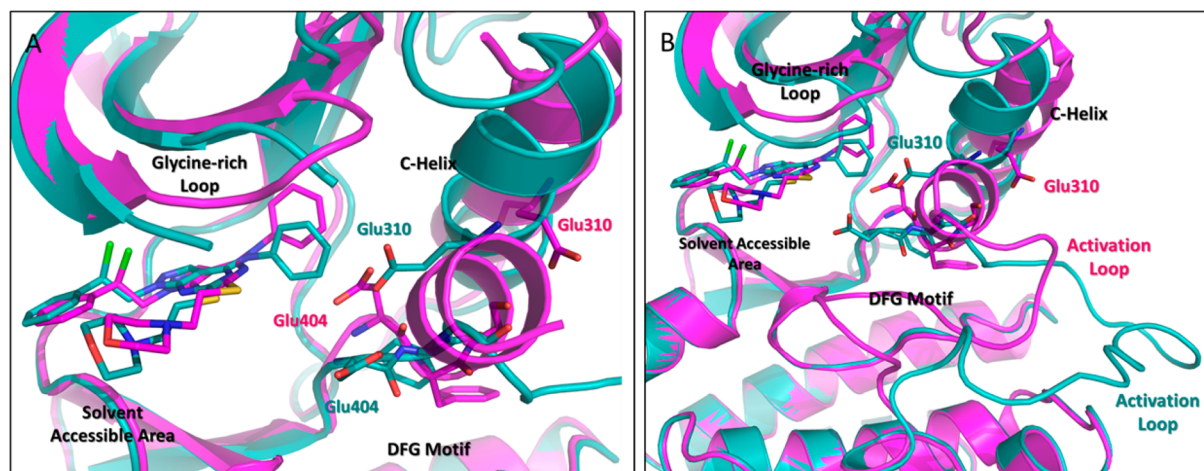

Figure 3. (A) Chains A (magenta) and B (aquamarine) of the crystal structure aligned each other. Differences between the two conformations were observed at the level of activation loop, αC-helix and P-loop. (B) Chains A (magenta) and B (aquamarine) used for the MC/FEP calculations. Missing residues in crystal structure were modeled.

Table 2. MC/FEP Results for the Change in Free Energy of Binding upon Introduction of Chlorine, Bromine, Fluorine, and Hydroxyl Substituents at the C4 Anilino Ring within Chain B
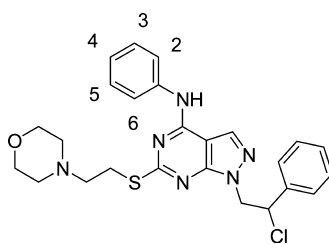
	OH to H $\Delta\Delta G_b$	σ	Cl to H $\Delta\Delta G_b$	σ	Br to H $\Delta\Delta G_b$	σ	F to H $\Delta\Delta G_b$	σ
C2	5.11	±0.10	4.8	±0.11	1.28	±0.11	1.96	±0.05
C3	4.89	±0.11	−5.37	±0.09	−6.67	±0.11	0.25	±0.03
C4	1.49	±0.13	−6.73	±0.09	−9.33	±0.10	−3	±0.05
C5	−6.68	±0.12	−8.36	±0.21	−8.71	±0.27	−3.66	±0.08
C6	−5.08	±0.09	−1.05	±0.07	−5.43	±0.11	0.71	±0.05

[a]$\Delta\Delta G_b$ is the computed change in free energy of binding (kcal/mol) for introducing the substituents; ±σ is the computed uncertainty.

Table 3. MC/FEP Results for the Change in Free Energy of Binding upon Introduction of Chlorine, Bromine, Fluorine, and Hydroxyl Substituents at the C4 Anilino Ring within Chain A
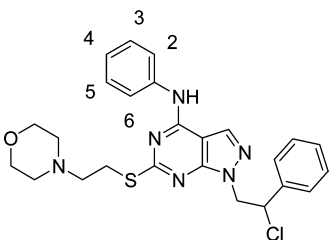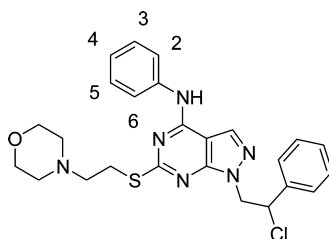

	OH to H $\Delta\Delta G_b$	σ	Cl to H $\Delta\Delta G_b$	σ	Br to H $\Delta\Delta G_b$	σ	F to H $\Delta\Delta G_b$	σ
C2	−1.96	±0.08	−2.47	±0.13	−3.47	±0.14	0.49	±0.05
C3	−9.41	±0.10	−2.70	±0.16	−4.58	±0.18	−3.78	±0.06
C4	−11.23	±0.08	−6.77	±0.13	−12.79	±0.20	−1.55	±0.06
C5	−7.51	±0.17	−12.14	±0.19	−10.77	±0.15	−2.89	±0.10
C6	0.06	±0.13	−6.83	±0.19	−11.03	±0.16	−6.48	±0.07

[a]$\Delta\Delta G_b$ is the computed change in free energy of binding (kcal/mol) for introducing the substituents; ±σ is the computed uncertainty.

the αC-helix (aa 303−318) and in the glycine-rich loop conformation (aa 273−281) (Figure 3A). In particular, in chain A, the Glu310 side chain projects away from the ATP binding site adopting a conformation similar to the closed and inhibited one of c-Src phosphorylated on Tyr527 (PDB code: 2SRC).[26] On the contrary, in chain B, Glu310 displays its side chain turned toward the active site, forming a salt bridge with Lys295. Moreover, in chain A, the solved amino acids of activation loop (Phe405−Asp413) are arranged in a three-turn α helix in a similar although not identical way as in 2SRC[27] phosphorylated c-Src. Vice versa, the determined activation loop of chain B recalls the one solved in the 1Y57[28] crystal structure. Another significant difference between chains A and B resides in the orientation of the DFG motif: in chain A, Glu404 projects its side chain deeply into the ATP binding site, thereby reducing the size of the hydrophobic pocket I which harbors the C4 substituent. Structural plasticity of c-Src in the presence of small molecule inhibitors was recently described.[29] To take into account the conformational differences, both chains were used in all the subsequent computational studies. A molecular modeling protocol was first applied to fill the missing residues (see Experimental Section for details), and the two refined chains were aligned to each other (Figure 3B). Starting from these completed structures, the optimization of **3** was pursued

using a computationally driven approach, primarily guided by results of Monte Carlo free-energy perturbation (MC/FEP) calculations.[30] Notably, although the racemic mixture of **3** was used for the preparation of the X-ray crystal structure, solely the *R*-enantiomer was found to be able to bind within the kinase active site in both the chains, pushing our studies toward further investigation on the chiral center. No differences were observed in the activities of the two enantiomers against c-Src (see in vitro biological activity paragraph below, Table 1). Next, we focused our attention on the C4 anilino ring with the aim of optimizing the activity of **3** by increasing the affinity for the c-Src kinase. MC/FEP halogen (chlorine, bromine, and fluorine) and hydroxyl scans were performed to identify the most promising sites and groups for substitutions of C4 anilino hydrogens. In the present calculations, *ortho* positions 2,6 and *meta* positions 3,5 are not equivalent as they do not interconvert during the MC runs requiring separate simulations for each conformer. According to the ring numbering in Table 2, replacement of hydrogen by OH was predicted to be favorable ($\Delta\Delta G_b$ represents the predicted change in free energy of binding for the OH to H perturbation, thus a positive value indicates that OH is preferred over H) by 5.11, 4.89, 1.49 kcal/mol at C2, C3, and C4, respectively, and unfavorable at C5 and C6 ($\Delta\Delta G_b$ of −6.68 and −5.08 kcal/mol, respectively)

Table 4. Halogen Bond Scanning for Chlorine and Bromine Atoms in Both Chain A and Chain B

	chain A				chain B			
	Br$^\sigma$ to Br ($\Delta\Delta G_b$)	σ	Cl$^\sigma$ to Cl ($\Delta\Delta G_b$)	σ	Br$^\sigma$ to Br ($\Delta\Delta G_b$)	σ	Cl$^\sigma$ to Cl ($\Delta\Delta G_b$)	σ
C3	−1.66	±0.10	−3.42	±0.06	−1.67	±0.03	−0.89	±0.03
C5	−0.89	±0.06	−0.79	±0.05	**0.35**	±0.03	**1.14**	±0.05

$^a\Delta\Delta G_b$ is the computed change in free energy of binding (kcal/mol) for introducing the substituents; $\pm\sigma$ is the computed uncertainty.

when initial complexes were built using chain B. Positive $\Delta\Delta G_b$ values were also found with the introduction of chlorine, bromine, or fluorine at C2 (4.8, 1.28, and 1.96 kcal/mol, respectively). On the contrary, in chain A, the entity of these substituents resulted to be unfavorable with negative $\Delta\Delta G_b$ (Table 3). Taking into account the MC/FEP results, a focused library of pyrazolo[3,4-*d*]pyrimidine derivatives bearing a *m*-OH substituent at the C4 anilino ring was synthesized in order to increase both water solubility and c-Src binding affinities of compounds under study. Furthermore, analogues substituted with bromine, chlorine, and fluorine in *meta* position were also synthesized and tested in enzymatic assays to enlarge the structure−activity relationships (Table 1) despite the prediction of unfavorable outcomes. Concerning these last substitutions, the possibility of halogen bonding between our inhibitors and the ATP binding site was also investigated by halogen bond scanning on both chain A and B considering *m*-Br and *m*-Cl substituents. To this aim, the enhanced force field OPLS/CM1Ax was employed in which the halogen representation has been modified to incorporate halogen bonding with the addition of the partial positive charge which represents the σ hole.[31] FEP results then predicted the relative free energies of binding from the modified halogen atom type to the classic one (namely Br$^\sigma$ to Br and Cl$^\sigma$ to Cl, Table 4). A marginal effect of halogen bond interaction was found for chlorine and bromine substituents at C5 position during chain B simulations (1.14 and 0.35 kcal/mol, respectively), while negative results were obtained in case of using chain A. The calculated positive contribution of halogen bonding was due to the interaction of Cl or Br with the carbonyl backbone of Ile336, working as Lewis base. However, this contribution has only limited effect on the total free energy of binding calculated for the introduction of bromine or chlorine at the *meta* position of C4 anilino group, which still remains generally negative. In summary, analysis of the MC/FEP results clearly highlighted that c-Src binding affinity may be enhanced by introducing a hydroxyl group at position 3 of C4 anilino ring, which allows for the stabilization of the complex between the chain B conformation of c-Src and the pyrazolo[3,4-*d*]pyrimidine derivatives. The hydrogen-bond interaction between the 3-OH of the ligand and the Glu310 side chain, usually involved in the formation of a salt bridge with Lys295, undoubtedly gives an important contribution to the binding affinity. This interaction was not possible in chain A because of the different orientation of the Glu310 side chain which points out from the active site (Figure 4). On the other hand, the introduction of an

hydroxyl group or halogens at position 2 were also predicted as favorable and will thus be subjected to our future studies.
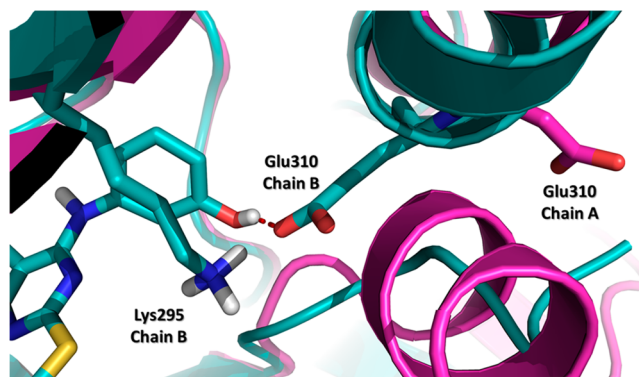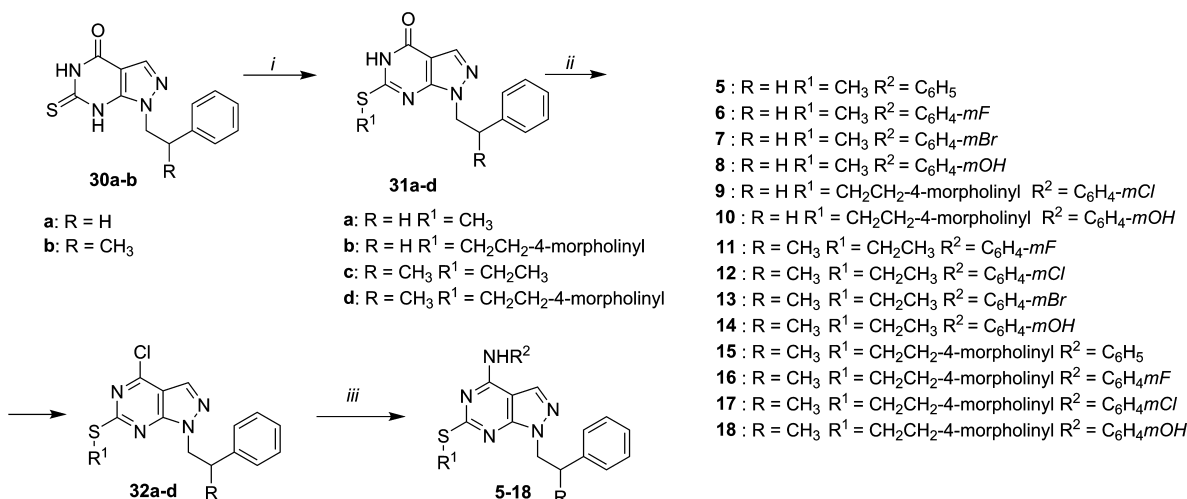

Figure 4. Hydrogen-bond between the 3-OH of the ligand and the Glu310 of chain B (aquamarine) is highlighted with red dashed line. The orientation of Glu310 side-chain in chain A (magenta) is also visualized.
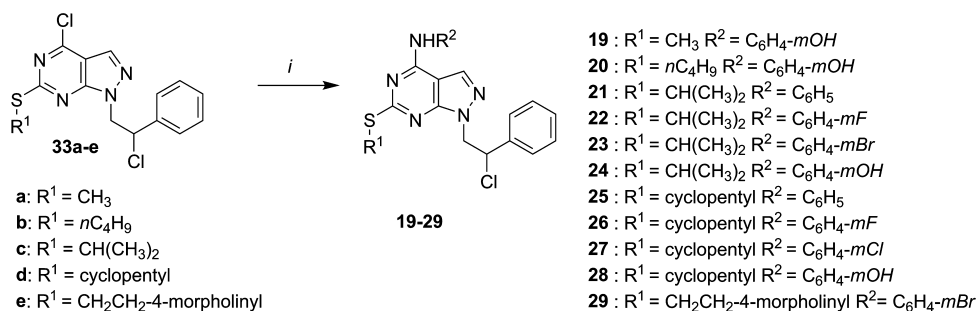
Chemistry. The synthesis of compounds **5**−**18** is reported in Scheme 1. Alkylation of the thiocarbonyl group of derivatives **30a**−**b**[25] with iodomethane, iodoethane, or 4-(2-chloroethyl)-morpholine afforded the 6-alkylthio derivatives **31a**−**d**, which were in turn treated with the Vilsmeier complex (POCl$_3$/DMF, 1:1) in CH$_2$Cl$_2$ at reflux for 6−8 h to obtain compounds **32a**−**d** bearing a chlorine atom in C4. Finally, reaction of **32a**−**d** with the suitable anilines in absolute ethanol at reflux for 3−5 h gave desired compounds **5**−**18** in good yields.

The synthesis of compounds **19**−**29** was performed starting from intermediates **33a**−**e** already reported by us (Scheme 2).[22,26,32] The suitable 4-chloro derivatives **33a**−**e** were reacted with the proper aniline in absolute ethanol at reflux for 3−5 h to give desired compounds **19**−**29** with good yields.

In Vitro Biological Activity. All synthesized compounds, including reference compound **3**, were initially tested in a cell-free assay (see Experimental Section) to evaluate their affinity toward isolated c-Src (Table 1). Compounds **4**, **5**, **8**, and **27** already published by us[26,33,34] have been also inserted in Table 1 for comparison purpose. First, to characterize the biological profile of each enantiomer, the racemic mixture of **3** was resolved by semipreparative HPLC (see Supporting Information, Figure S1−S2), thus obtaining each single optically pure entity (**3-R** and **3-S**) with high enantiomeric excess (>98%). Compounds **3-R** and **3-S** were then submitted to biological

Scheme 1. Preparation of Derivatives 5–18[a]

30a-b

a: R = H
b: R = CH₃

i →

31a-d

a: R = H R¹ = CH₃
b: R = H R¹ = CH₂CH₂-4-morpholinyl
c: R = CH₃ R¹ = CH₂CH₃
d: R = CH₃ R¹ = CH₂CH₂-4-morpholinyl

ii →

5 : R = H R¹ = CH₃ R² = C₆H₅
6 : R = H R¹ = CH₃ R² = C₆H₄-*mF*
7 : R = H R¹ = CH₃ R² = C₆H₄-*mBr*
8 : R = H R¹ = CH₃ R² = C₆H₄-*mOH*
9 : R = H R¹ = CH₂CH₂-4-morpholinyl R² = C₆H₄-*mCl*
10 : R = H R¹ = CH₂CH₂-4-morpholinyl R² = C₆H₄-*mOH*
11 : R = CH₃ R¹ = CH₂CH₃ R² = C₆H₄-*mF*
12 : R = CH₃ R¹ = CH₂CH₃ R² = C₆H₄-*mCl*
13 : R = CH₃ R¹ = CH₂CH₃ R² = C₆H₄-*mBr*
14 : R = CH₃ R¹ = CH₂CH₃ R² = C₆H₄-*mOH*
15 : R = CH₃ R¹ = CH₂CH₂-4-morpholinyl R² = C₆H₅
16 : R = CH₃ R¹ = CH₂CH₂-4-morpholinyl R² = C₆H₄*mF*
17 : R = CH₃ R¹ = CH₂CH₂-4-morpholinyl R² = C₆H₄*mCl*
18 : R = CH₃ R¹ = CH₂CH₂-4-morpholinyl R² = C₆H₄*mOH*

32a-d

iii →

5-18

[a]Reagents and conditions: (i) Method A, CH₃I, anhyd THF, reflux, 12 h (for **31a**); method B, 4-(2-chloroethyl)morpholine, NaOH, EtOH, anhyd DMF, reflux, 6 h (for **31b** and **31d**); method C, C₂H₅I, K₂CO₃, anhyd DMF, rt, 20 h (for **31c**). (ii) POCl₃/DMF, CH₂Cl₂, reflux, 6–8 h. (iii) R²NH₂, EtOH, reflux, 3–5 h.

Scheme 2. Preparation of Derivatives 19–29[a]

33a-e

a: R¹ = CH₃
b: R¹ = *n*C₄H₉
c: R¹ = CH(CH₃)₂
d: R¹ = cyclopentyl
e: R¹ = CH₂CH₂-4-morpholinyl

i →

19-29

19 : R¹ = CH₃ R² = C₆H₄-*mOH*
20 : R¹ = *n*C₄H₉ R² = C₆H₄-*mOH*
21 : R¹ = CH(CH₃)₂ R² = C₆H₅
22 : R¹ = CH(CH₃)₂ R² = C₆H₄-*mF*
23 : R¹ = CH(CH₃)₂ R² = C₆H₄-*mBr*
24 : R¹ = CH(CH₃)₂ R² = C₆H₄-*mOH*
25 : R¹ = cyclopentyl R² = C₆H₅
26 : R¹ = cyclopentyl R² = C₆H₄-*mF*
27 : R¹ = cyclopentyl R² = C₆H₄-*mCl*
28 : R¹ = cyclopentyl R² = C₆H₄-*mOH*
29 : R¹ = CH₂CH₂-4-morpholinyl R²= C₆H₄-*mBr*

[a]Reagents and conditions: (i) R²NH₂, EtOH, reflux, 3–5 h.

evaluation in a cell-free assay. Comparable K_i values were found for the two enantiomers (K_i values of 0.20 and 0.23 μM for **3-R** and **3-S**, respectively). Accordingly, the remaining synthesized compounds were tested as racemic mixture. Still focusing on the chiral center, the chlorine substitution determined an improvement of the activity against c-Src (compare **4** with **9** and **17**). On the other hand, as it can be appreciated from Table 1, the rationally designed derivatives **10**, **18**, **19**, **24**, and **28** showed potent in vitro inhibitory effect against c-Src with K_i values in the low nanomolar range (40, 70, 30, 10, and 7 nM, respectively). These potencies were most likely evoked due to the contribution of the hydroxyl group in *meta* position of the anilino ring, as hypothesized by our molecular modeling calculations and further confirmed by the observed structure−activity relationships. With the simple addition of a *m*-OH substituent on the C4 anilino ring, potent agents were identified with 2−30-fold increased activities (compare **8** with **5**, **18** with **15**, **24** with **21**, and **28** with **25** in Table 1). On the contrary, no clear trends were observed with the introduction of fluorine, chlorine, or bromine at the same position. However, compounds with remarkable activities were identified also in these series such as **13**, **26**, and **29**, showing K_i values of around 100 nM. Biological results on halogen derivatives were in contrast to the expectation from the computed $\Delta\Delta G$ values. A feasible explanation for this discrepancy may be due to the fact

that ligand-induced conformational changes are much more pronounced than those explored by Monte Carlo because of the lack of sampling of the protein backbone whose atoms are frozen during the simulations. The most active c-Src inhibitors **10**, **18**, **19**, **24**, and **28** were also tested against Abl. These compounds maintained the dual Src/Abl inhibitory profile of lead structures **3** and **4** but showed K_i values of 1 order of magnitude higher than for Src, possessing a significant selectivity for c-Src over Abl. Selected c-Src inhibitors were then evaluated for their ability to inhibit the proliferation of neuroblastoma SH-SY5Y cells by spheroid formation assay. Cells were treated for 72 h with increasing concentrations of the inhibitors (0.01−50 μM), and IC₅₀ values were calculated considering the mean area of spheroids respect to control (Table 1). The strongest effect on SH-SY5Y was obtained by **19** and **29** that showed IC₅₀ values of 0.12 and 0.34 μM, respectively. The growth rate of spheroids in the presence of **29** and representative images are shown in Supporting Information (Figure S3).

It is noteworthy, from the structure−activity relationships (SAR) analysis, two moieties reported in literature as toxicophoric groups, the phenol and the alkyl halide, emerged as crucial for the activity. To evaluate the nonspecific cytotoxic effect of **19** and **29**, we treated in vitro normal embryonic fibroblasts Wi38 with increasing doses of the drugs. **19** and **29**

affected Wi38 cell viability starting from concentration greater than 100 μM.

Biological effect of **29** was also evaluated through analysis of cell cycle (Figure 5). SH-SY5Y cells were treated with
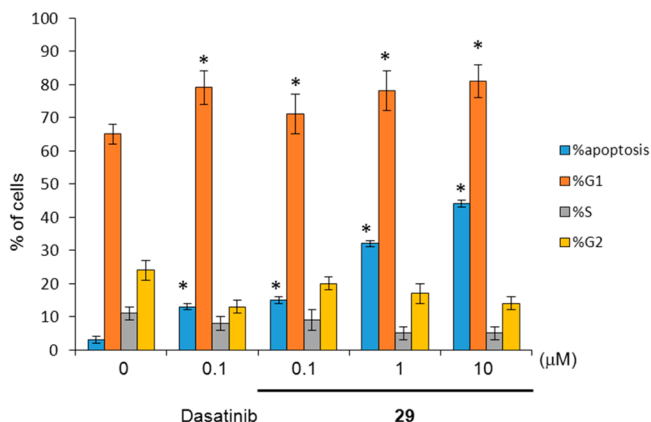

Figure 5. Analysis of the cell cycle distribution of SH-SY5Y cells after treatment with increasing concentrations of **29** and in comparison with 0.1 μM Dasatinib. SH-SY5Y cells status was investigated by cytofluorimetry after propidium iodide staining, and results were expressed as percentage of cells in each phase of cell cycle respect to total viable cells. Apoptosis was evaluated by calculating the number of hypodiploid cells and was expressed as percentage of apoptotic cells respect to total cells (viable and dead cells). Results are the mean of three different experiments. *$p < 0.01$ respect the value of the untreated cells.

increasing concentration of **29** (0.1−10 μM), and the percentage of cells in each phase of cell cycle was evaluated by cytofluorimetric analysis of DNA content. **29** determined a significant and dose-dependent accumulation of cells in the G1 phase of cell cycle starting from 0.1 μM. In parallel we observed a progressive accumulation of hypodiploid cells, indicating the presence of apoptotic cells. The comparison with the reference compound Dasatinib at 0.1 μM demonstrated that the biological effect by **29** was not significantly different with respect to cytotoxic effect by Dasatinib. The treatment with 10 μM **29** induced the apoptosis in about 50% of treated cells.

ADME Studies. It is well-known that kinase inhibitors are generally affected by solubility issues because of their lipophilic nature. Therefore, the early evaluation of ADME properties in this field represents, more than ever, a key step to guide the

drug candidate selection. Accordingly, in vitro ADME studies were conducted on the most potent c-Src inhibitors reported herein in order to early assess their absorption/stability. In particular, aqueous solubility, parallel artificial membrane permeability (PAMPA), and human liver microsomes (HLM) stability were evaluated for the most active c-Src inhibitors (Table 1). Overall, optimal ADME properties were measured for the entity of studied compounds. Indeed, the metabolic stability was found to be higher than 90% and membrane permeability values ranged from 1.72 to 9.33 × 10^{-6} cm/s, highlighting a sufficient ability to cross the cell membranes. Furthermore, water solubility of some compounds was increased by about 2- to greater than 57-fold compared to that of reference **3**, with the more soluble compound **10** showing a solubility value of 97 μg/mL.

In Vivo Studies. Among the most promising c-Src inhibitors, compound **29** was selected for the in vivo studies because it showed an appropriate balance of different ADME properties, remarkable activity in the cell-free assay, and promising submicromolar potency against SH-SY5Y neuroblastoma cells. The anticancer activity of **29** was tested in vivo using a xenograft mouse model. Mice inoculated with SH-SY5Y neuroblastoma cells were treated daily with 50 mg/kg **29** starting from the appearance of a visible tumor mass, and the tumor volume was evaluated at regular intervals. **29** caused a significant reduction in tumor volume after 60 days of oral treatment with a reduction of more than 50% in mean tumor volume compared to placebo treated mice (Figure 6A). Remarkably, mice did not show signs of distress or weight loss. In vivo Dasatinib treatment (50 mg/kg) determined a very similar inhibitory trend, but the appearance of palpable tumor masses was earlier in Dasatinib group with respect to mice treated with **29**. It is notable that the tumor associated angiogenesis at the end point was significantly compromised in mice treated with **29** (data not shown). Thus, a three-dimensional in vitro sprouting assay was performed to analyze the effect of **29** on angiogenic response of endothelial cells. Spheroids from endothelial HBMECs were seeded on Matrigel. Twenty-four hours after the beginning of the experiment, we observed a significant reduction of angiogenesis as demonstrated by the reduction of the number of sprouts derived from spheroid treated with the compound, at 0.5 and 1 μM concentrations, compared with untreated cells (Figure 6B).
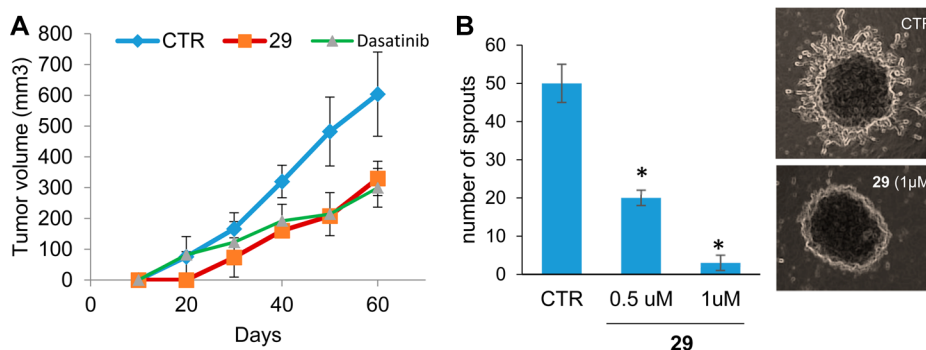

Figure 6. Evaluation of antitumoral effect of **29** and of reference compound Dasatinib. (A) Inhibition of tumor growth by 50 mg/kg **29** or 50 mg/kg Dasatinib treatment in a rodent model of neuroblastoma. Tumor xenografts were monitored measuring the diameters of tumor mass. (B) Antiangiogenic effect of **29** evaluated by sprouting assay with endothelial cells. Histogram shows the mean number of sprouts per spheroid for each experimental condition (CTR = untreated cells). Representative images are shown on the right. *$p < 0.01$ according Student-t test.

CONCLUSIONS

In summary, for the first time an X-ray crystal structure of c-Src in complex with one of our patented prazolo[3,4-*d*]pyrimidines was obtained in good resolution. The solved structure confirmed the binding mode previously predicted by us for C6-substituted derivatives within the ATP binding site of c-Src. Starting from this crystal structure, a computationally driven hit-to-lead optimization primarily guided by results of free-energy perturbations was successfully conducted, leading to the identification of novel derivatives with improved potencies against c-Src. A hydroxyl group at the *meta* position of the C4 aniline ring was identified as the key structural feature for the inhibitory activity toward c-Src. The *m*-OH group was predicted to be efficient in establishing hydrogen-bond interaction with the conserved residue Glu310. This polar interaction was already proposed as crucial for the development of potent c-Src inhibitors.[35] In this regard, our results are also in line with, and reinforce, this finding. It is noteworthy that the introduction of the hydroxyl group further led to a beneficial effect in terms of water solubility which was increased by 10 or more fold with respect to the starting hit. Furthermore, on the basis of the knowledge that the tyrosine kinase c-Src is overexpressed or hyperactivated in many solid cancers, including NB, the antitumor activity of the optimized pyrazolo[3,4-*d*]pyrimidines reported herein was assessed by measuring their effect on SH-SY5Y NB cell proliferation. The most promising agents inhibited cell viability with IC$_{50}$ values in the submicromolar range. Next, to test the efficacy in vivo, SH-SY5Y cells were subcutaneously injected in nude mice and drug treatment conducted until day 60. Tumor growth was significantly inhibited by compound **29** at the dose of 50 mg/kg. Subsequent observations on excised tumor masses and in vitro assays suggest that c-Src inhibitor was active on both cancer cells and tumor-associated endothelial cells inhibiting their migratory capacity and angiogenesis. Overall, these results illustrated how the combination of structural analysis, computational studies, organic chemistry, and biological experiments in vitro and in vivo can be effectively utilized to develop anticancer agents active against neuroblastoma.

EXPERIMENTAL SECTION

Crystallization and Structure Determination of c-Src-3. Inhibitor **3** was cocrystallized with c-Src using conditions similar to those previously reported by Michalczyk et al.[36] Briefly, final concentrations of 540 μM inhibitor (100 mM stock in DMSO) and 180 μM wild-type c-Src (stored in 50 mM Tris pH 8.0, 100 mM NaCl, 1 mM DTT, 5% glycerol (v/v)) were preincubated for 1 h on ice to form the enzyme−inhibitor complex prior to crystallization. Crystals were grown using the hanging drop method at 20 °C after mixing 1 μL of protein−inhibitor solution with 1 μL of reservoir solution (0−30 mM NaCl, pH 7.0, 9−20% ethylene glycol). All crystals were frozen with further addition of 30% (v/v) glycerol. Diffraction data of the c-Src−**3** complex crystals were collected at the PX10SA beamline of the Swiss Light Source (PSI, Villingen, Switzerland) to a resolution of 2.1 Å, using wavelengths close to 1 Å. The data set was processed with XDS[2] and scaled using XSCALE.[37,38]

Structure Determination and Refinement of c-Src-3. The c-Src−inhibitor complex structure was solved by molecular replacement with PHASER[39] using the published c-Src structure 2OIQ[40] as template. The two c-Src molecules in the asymmetric unit were manually modified using the program COOT.[41] The model was first refined with CNS[42] using simulated annealing to remove model bias. The final refinement was performed with REFMAC5.[43] Inhibitor topology files were generated using the Dundee PRODRG2 server.[44] Refined structures were validated with PROCHECK.[45] Detailed data,

refinement, and Ramachandran statistics are provided in Supporting Information (Table S1).

Computer Modeling. *Loops Modeling Protocol.* The FASTA sequence of c-Src was used as query, the coordinates of the two chains of our crystal structure (c-Src in complex with **3**) were in turn employed as templates and the missing residues were built by using the program Prime.[46] For each chain, the serial loop sampling approach was applied by choosing "Extended" as level of accuracy (recommended for loop length between 6 and 11 residues) and the lowest energy conformation was saved for the next analysis. Similarly, Prime was used to fill the A-loop of the chain B by the building of the Cys277 missing residue and to construct the amino acids 300 and 301 absent in the chain A.[47] The maximum number of structures to return was set to 10. An energy cutoff of 10 kcal/mol was applied. Loop conformations were clustered, and representatives of each cluster were selected. The best scoring loop structure was finally selected.

Monte Carlo/Free Energy Perturbation. MC/FEP calculations were performed with the MCPRO program and following standard protocols.[48,49] Z-Matrix for the c-Src−ligand complexes were obtained with the molecular growing program BOMB[48] starting from the pose of **3** within our crystal structure (PDB code: 4O2P). The models included the 160 amino acid residues nearest to the ligand. Short conjugate-gradient minimizations were carried out on the initial structures for all complexes to relieve any unfavorable contacts. Coordinates for the free ligands were obtained by extraction from the complexes. Next, 1500 steps of conformational search analysis was carried out on the ligands using BOSS[50] program with the OPLS/CM1A and OPLS/CM1Ax force fields and GB/SA hydration. The resultant conformer with the lowest energy was used for FEP calculation. The unbound ligands and complexes were solvated with TIP4P water spheres ("caps") with a 25 Å radius. The water molecules in too close contact with solute atoms were removed. A few remote side chains were neutralized in order to maintain overall charged neutrality for each system. The ligand and the protein side chains within 10 Å of any ligand were sampled during the MC simulations. The only constraints were the bond lengths in side chains, and all backbone atoms were frozen after a short conjugate-gradient minimization. The energetics for the systems were evaluated with the OPLS-AA and OPLS-AAx force fields for the protein and OPLS/CM1A and OPLS/CM1Ax force fields for ligands.[31] The CM1A atomic charges were scaled by 1.14 for neutral molecules. Differences in free energies of binding were determined from the usual thermodynamic cycle that requires conversion of one ligand to another both free in water and bound to the protein. The FEP calculations utilized 11 windows of simple overlap sampling. For the unbound ligand, each window consisted of 40 M configurations of equilibration and 60 M configurations for averaging. For the bound calculations, each window covered 20 M configurations of solvent only equilibration, 40 M configurations of full equilibration, and 50 M configurations of averaging. In the case of halogen bond scanning, the number of configurations was increased to 60 M of equilibration and 80 M of averaging. All MC simulations were run at 298 K.

Chemistry. Starting materials were purchased from Aldrich-Italia (Milan, Italy). Melting points were determined with a Büchi 530 apparatus and are uncorrected. IR spectra were measured in KBr or CHCl$_3$ with a PerkinElmer 398 spectrophotometer. ^{1}H NMR spectra were recorded at 400 MHz in CDCl$_3$ or [D$_6$]DMSO on a Bruker Avance DPX400 spectrometer. Chemical shifts are reported as δ (ppm) relative to TMS as the internal standard, *J* in Hz. ^{1}H patterns are described using the following abbreviations: s = singlet, d = doublet, t = triplet, q = quartet, quint = quintet, sx = sextet, sept = septet, m = multiplet, and br s = broad singlet. TLC was carried out using Merck TLC plates silica gel 60 F254. Chromatographic purifications were performed on columns packed with Merck 60 silica gel, 230−400 mesh, for flash technique. Elemental analyses (Supporting Information, Table S2) were determined with an elemental analyzer EA 1110 (Fison-Instruments, Milan, Italy), and the purity of all synthesized compounds was >95%. Analyses for C, H, N, and S were within ±0.3% of the theoretical value. Mass spectra (MS) data were obtained using an Agilent 1100 LC/MSD VL system

(G1946C) with a 0.4 mL/min flow rate using a binary solvent system of 95:5 methanol/water. UV detection was monitored at 254 nm. MS were acquired in positive and negative modes, scanning over the mass range 50−1500. The following ion source parameters were used: drying gas flow, 9 mL/min; nebulizer pressure, 40 psig; drying gas temperature, 350 °C.

Compounds **4**, **5**, **8**, and **27** and intermediates **30a,b**, **31a**, **32a**, and **33a−e** were already reported by us.[21,23,25,30,32]

*General Procedure for the Synthesis of Compounds **31b** and **31d**.* A mixture of 1-substituted 6-thioxo-1,5,6,7-tetrahydro-4*H*-pyrazolo[3,4-*d*]pyrimidin-4-one **30a,b** (1 mmol), 4-(2-chloroethyl)-morpholine (224 mg, 1.5 mmol), NaOH (40 mg, 1 mmol) in anhydrous DMF (1 mL), and absolute ethanol (3 mL) was stirred at reflux for 6 h. After cooling to room temperature, the solvent was evaporated under reduced pressure and the mixture was poured into cold water (20 mL). The obtained solid was filtered, washed with water, and recrystallized from absolute ethanol.

*6-[2-Morpholin-4-ylethyl)thio]-1-(2-phenylethyl)-1,5-dihydro-4H-pyrazolo[3,4-d]pyrimidin-4-one (**31b**).* White solid (197 mg, 51%); mp 197−198 °C. ^{1}H NMR (CDCl$_3$): δ 2.55−2.70 (m, 4H, 2CH$_2$N morph), 2.80−2.84 (m, 2H, CH$_2$N), 3.17−3.24 (m, 4H, CH$_2$S + CH$_2$Ar), 3.80−3.85 (m, 4H, 2CH$_2$O morph), 4.50 (t, *J* = 7.6 Hz, 2H, CH$_2$N pyraz), 7.10−7.26 (m, 5H Ar), 8.02 (s, 1H, H-3). IR (cm^{-1}): 3500−2800 (NH), 1667 (CO). MS: *m/z* [M + 1]$^+$ 386. Anal. (C$_{19}$H$_{23}$N$_5$O$_2$S) C, H, N, S.

*6-[2-Morpholin-4-ylethyl)thio]-1-(2-phenylpropyl)-1,5-dihydro-4H-pyrazolo[3,4-d]pyrimidin-4-one (**31d**).* White solid (200 mg, 50%); mp 128−130 °C. ^{1}H NMR (CDCl$_3$): δ 1.24 (d, *J* = 6.8 Hz, 3H, CH$_3$), 2.60−2.70 (m, 4H, 2CH$_2$N morph), 2.80−2.90 and 3.15−3.25 (2m, 4H, SCH$_2$CH$_2$), 3.45−3.52 (m, 1H, CHCH$_3$), 3.80−4.00 (m, 4H, 2CH$_2$O morph), 4.38−4.40 (m, 2H, CH$_2$N pyraz), 7.18−7.28 (m, 5H Ar), 7.99 (s, 1H, H-3). IR (cm^{-1}): 3450−2900 (NH), 1678 (CO). MS: *m/z* [M + 1]$^+$ 400. Anal. (C$_{20}$H$_{25}$N$_5$O$_2$S) C, H, N, S.

*Synthesis of 6-(Ethylthio)-1-(2-phenylpropyl)-1,5-dihydro-4H-pyrazolo[3,4-d]pyrimidin-4-one **31c**.* A mixture of 1-(2-phenyl-propyl)-6-thioxo-1,5,6,7-tetrahydro-4*H*-pyrazolo[3,4-*d*]pyrimidin-4-one **30b** (286 mg, 1 mmol), iodoethane (172 mg, 1.1 mmol), and K$_2$CO$_3$ (138 mg, 1 mmol) in anhydrous DMF (2 mL) was stirred at room temperature for 20 h. The mixture was poured into cold water (50 mL). The obtained solid was filtered, washed with water, and recrystallized from absolute ethanol. White solid (192 mg, 61%); mp 155−156 °C. ^{1}H NMR ([D$_6$]DMSO): δ 1.22 (d, *J* = 7.0 Hz, 3H, CH$_3$CH), 1.36 (t, *J* = 7.2, 3H, SCH$_2$CH$_3$), 3.17 (q, *J* = 7.2 Hz, 2H, SCH$_2$), 3.40−3.50 (m, 1H, CHCH$_3$), 4.26−4.50 (m, 2H, CH$_2$N), 7.07−7.30 (m, 5H Ar), 7.94 (s, 1H, H-3), 12.10 (br s, 1H, NH disappears with D$_2$O). IR cm^{-1}: 3110−2800 (NH), 1681 (CO). MS: *m/z* [M + 1]$^+$ 315. Anal. (C$_{16}$H$_{18}$N$_4$OS) C, H, N, S.

*General Procedure for the Synthesis of Compounds **32b−d**.* The Vilsmeier complex, previously prepared from POCl$_3$ (0.74 mL, 8 mmol) and anhydrous DMF (590 mg, 8 mmol) was added to a suspension of **31b−d** (1 mmol) in CH$_2$Cl$_2$ (10 mL). The mixture was refluxed for 6−8 h. For compounds **32b** and **32d**, the solution was washed with a 4N NaOH solution (2 × 10 mL) and water (2 × 10 mL), dried (MgSO$_4$), filtered, and concentrated under reduced pressure. For compound **32c**, the solution was washed with water (2 × 10 mL), dried (MgSO$_4$), filtered, and concentrated under reduced pressure. The crude oil was purified by column chromatography (Florisil, 100−200 mesh), using diethyl ether as the eluent, to afford the pure product.

*4-Chloro-6-[(2-morpholin-4-ylethyl)thio]-1-(2-phenylethyl)-1H-pyrazolo[3,4-d]pyrimidine (**32b**).* Yellow oil (323 mg, 80%). ^{1}H NMR (CDCl$_3$): δ 2.51−2.90 (m, 6H, 2CH$_2$N morph + CH$_2$N), 3.22 (t, *J* = 7.2 Hz, 2H, CH$_2$Ar), 3.30−3.40 (m, 2H, SCH$_2$), 3.68−3.88 (m, 4H, 2CH$_2$O morph), 4.62 (t, *J* = 7.2 Hz, 2H, CH$_2$N pyraz), 7.09−7.26 (m, 5H Ar), 8.01 (s, 1H, H-3). MS: *m/z* [M + 1]$^+$ 405. Anal. (C$_{19}$H$_{22}$N$_5$OClS) C, H, N, S.

*4-Chloro-6-(ethylthio)-1-(2-phenylpropyl)-1H-pyrazolo[3,4-d]-pyrimidine (**32c**).* Yellow oil (300 mg, 90%). ^{1}H NMR (CDCl$_3$): δ 1.31 (d, *J* = 7.2 Hz, 3H, CH$_3$CH), 1.47 (t, *J* = 7.4 Hz, 3H, SCH$_2$CH$_3$), 3.21 (q, *J* = 7.4 Hz, 2H, SCH$_2$), 3.48−3.63 (m, 1H, CHCH$_3$), 4.42−

4.66 (m, 2H, CH$_2$N), 7.12−7.31 (m, 5H Ar), 8.01 (s, 1H, H-3). MS: *m/z* [M + 1]$^+$ 334. Anal. (C$_{16}$H$_{17}$N$_4$ClS) C, H, N, S.

*4-Chloro-6-[(2-morpholin-4-ylethyl)thio]-1-(2-phenylpropyl)-1H-pyrazolo[3,4-d]pyrimidine (**32d**).* Yellow oil (288 mg, 69%). ^{1}H NMR (CDCl$_3$): δ 1.22 (d, *J* = 6.8 Hz, 3H, CH$_3$), 2.50−2.66, 2.73−2.82, 3.26−3.41 and 3.45−3.58 (4m, 8H, 2CH$_2$N morph + SCH$_2$CH$_2$), 3.68−3.85 (m, 5H, 2CH$_2$O morph + CHCH$_3$), 4.40−4.56 (m, 2H, CH$_2$N pyraz), 7.07−7.30 (m, 5H Ar), 7.96 (s, 1H, H-3). MS: *m/z* [M + 1]$^+$ 419. Anal. (C$_{20}$H$_{24}$N$_5$OClS) C, H, N, S.

*General Procedure for the Synthesis of Compounds **6**, **7**, **9**, **11−13**, **15−17**, **21−23**, **25**, **26**, **29**.* The suitable aniline (2 mmol) was added to a solution of the 4-chloro derivative **32a−d** and **33a−e** (1 mmol) in absolute ethanol (5 mL), and the mixture was refluxed for 3−5 h. After cooling to room temperature, the obtained solid was filtered, washed with water, and recrystallized from absolute ethanol.

*N-(3-Fluorophenyl)-6-(methylthio)-1-(2-phenylethyl)-1H-pyrazolo[3,4-d]pyrimidin-4-amine (**6**).* White solid (220 mg, 58%); mp 133−135 °C. ^{1}H NMR (CDCl$_3$): δ 2.59 (s, 3H, SCH$_3$), 3.18 (t, *J* = 7.6 Hz, 2H, CH$_2$Ar), 4.57 (t, *J* = 7.6 Hz, 2H, CH$_2$N), 6.92−6.95 and 7.15−7.37 and 7.47−7.50 (3m, 10H, 9 Ar + H-3). IR (cm^{-1}): 3100−2500 (NH). MS: *m/z* [M + 1]$^+$ 381. Anal. (C$_{20}$H$_{18}$N$_5$FS) C, H, N, S.

*N-(3-Bromophenyl)-6-(methylthio)-1-(2-phenylethyl)-1H-pyrazolo[3,4-d]pyrimidin-4-amine (**7**).* White solid (273 mg, 62%); mp 233−234 °C. ^{1}H NMR (CDCl$_3$ + [D$_6$]DMSO): δ 2.50 (s, 3H, SCH$_3$), 3.12 (t, *J* = 7.6 Hz, 2H, CH$_2$Ar), 4.97 (t, *J* = 7.6 Hz, 2H, CH$_2$N), 7.04−7.19 and 7.59−7.61 (2m, 9H, H-3). IR (cm^{-1}): 2929 (NH). MS: *m/z* [M + 1]$^+$ 441. Anal. (C$_{20}$H$_{18}$N$_5$BrS) C, H, N, S.

*N-(3-Chlorophenyl)-6-[(2-morpholin-4-ylethyl)thio]-1-(2-phenyl-ethyl)-1H-pyrazolo[3,4-d]pyrimidin-4-amine (**9**).* White solid (233 mg, 47%); mp 235−237 °C. ^{1}H NMR (CDCl$_3$): δ 2.88−2.95 (m, 4H, 2CH$_2$N morph), 3.15 (t, *J* = 7.0 Hz, 2H, CH$_2$Ar), 3.22−3.30 (m, 2H, CH$_2$N), 3.69−3.74 (m, 2H, SCH$_2$), 4.00−4.49 (m, 4H, 2CH$_2$O morph), 4.64 (t, *J* = 7.0 Hz, 2H, CH$_2$N pyraz), 7.16−7.38 (m, 9H Ar), 7.51 (s, 1H, H-3). IR (cm^{-1}): 3300−3100 (NH). MS: *m/z* [M + 1]$^+$ 496. Anal. (C$_{25}$H$_{27}$N$_6$OClS) C, H, N, S.

*6-(Ethylthio)-N-(3-fluorophenyl)-1-(2-phenylpropyl)-1H-pyrazolo-[3,4-d]pyrimidin-4-amine (**11**).* White solid (208 mg, 51%); mp 133−135 °C. ^{1}H NMR (CDCl$_3$): δ 1.25 (d, *J* = 6.8 Hz, 3H, CH$_3$CH), 1.50 (t, *J* = 7.5 Hz, 3H, SCH$_2$CH$_3$), 3.20 (q, *J* = 7.5 Hz, 2H, SCH$_2$), 3.50−3.55 (m, 1H, CHCH$_3$), 4.39−4.51 (m, 2H, CH$_2$N), 6.91−6.95 and 7.08−7.49 (2m, 10H, 9 Ar + H-3). IR (cm^{-1}): 3290 (NH). MS: *m/z* [M + 1]$^+$ 409. Anal. (C$_{22}$H$_{22}$N$_5$FS) C, H, N, S.

*N-(3-Chlorophenyl)-6-(ethylthio)-1-(2-phenylpropyl)-1H-pyrazolo[3,4-d]pyrimidin-4-amine (**12**).* White solid (136 mg, 32%); mp 69−70 °C. ^{1}H NMR ([D$_6$]DMSO): δ 1.22 (d, *J* = 7.0 Hz, 3H, CH$_3$CH), 1.36 (t, *J* = 7.4 Hz, 3H, SCH$_2$CH$_3$), 3.18 (q, *J* = 7.4 Hz, 2H, SCH$_2$), 3.95−4.00 (m, 1H, CHCH$_3$), 4.29−4.45 (m, 2H, CH$_2$N), 7.11−8.15 (m, 10H, 9 Ar + H-3), 10.13 (br s, 1H, NH disappears with D$_2$O). IR (cm^{-1}): 3592 (NH). MS: *m/z* [M + 1]$^+$ 425. Anal. (C$_{22}$H$_{22}$N$_5$ClS) C, H, N, S.

*N-(3-Bromophenyl)-6-(ethylthio)-1-(2-phenylpropyl)-1H-pyrazolo[3,4-d]pyrimidin-4-amine (**13**).* White solid (192 mg, 41%); mp 83−84 °C. ^{1}H NMR (CDCl$_3$): δ 1.23 (d, *J* = 7.2 Hz, 3H, CH$_3$CH), 1.45 (t, *J* = 7.6 Hz, 3H, SCH$_2$CH$_3$), 3.19 (q, *J* = 7.6 Hz, 2H, SCH$_2$), 3.49−3.55 (m, 1H, CHCH$_3$), 4.39−4.50 (m, 2H, CH$_2$N), 7.16−7.46 (m, 9H Ar), 7.84 (s, 1H, H-3). IR cm^{-1}: 3300−3000 (NH). MS: *m/z* [M + 1]$^+$ 469. Anal. (C$_{22}$H$_{22}$N$_5$BrS) C, H, N, S.

*6-[2-Morpholin-4-ylethyl)thio]-N-phenyl-1-(2-phenylpropyl)-1H-pyrazolo[3,4-d]pyrimidin-4-amine (**15**).* White solid (332 mg, 70%); mp 212−213 °C. ^{1}H NMR (CDCl$_3$): δ 1.14 (d, *J* = 6.8 Hz, 3H, CH$_3$), 2.80−3.00 (m, 2H, SCH$_2$), 3.20−3.45, 3.46−3.60, 3.72−3.85 and 4.02−4.15 (4m, 11H, 4CH$_2$ morph + CH$_2$N + CHCH$_3$), 4.30−4.44 (m, 2H, CH$_2$N pyraz), 6.70−6.81 and 7.07−7.35 (2m, 10H Ar), 7.49 (s, 1H, H-3). IR (cm^{-1}): 3500−2800 (NH). MS: *m/z* [M + 1]$^+$ 476. Anal. (C$_{26}$H$_{30}$N$_6$OS) C, H, N, S.

*N-(3-Fluorophenyl)-6-[(2-morpholin-4-ylethyl)thio]-1-(2-phenyl-propyl)-1H-pyrazolo[3,4-d]pyrimidin-4-amine (**16**).* White solid (182 mg, 37%); mp 236−237 °C. ^{1}H NMR (CDCl$_3$): δ 1.24 (d, *J* = 7.0 Hz, 3H, CH$_3$), 2.08−2.60, 2.78−3.17, 3.27−3.74 and 3.97−4.38 (4m, 13H, SCH$_2$ + 4CH$_2$ morph + CH$_2$N + CHCH$_3$), 4.40−4.50 (m, 2H, CH$_2$N

pyraz), 5.90–6.40 and 7.03–7.50 (2m, 10H, 9 Ar + H-3), 9.33 (br s, 1H, NH, disappears with D_2O). IR (cm^{-1}): 3450–3100 (NH). MS: m/z [M + 1]$^+$ 494. Anal. ($C_{26}H_{29}N_6OFS$) C, H, N, S.

N-(3-Chlorophenyl)-6-[(2-morpholin-4-ylethyl)thio]-1-(2-phenyl-propyl)-1H-pyrazolo[3,4-d]pyrimidin-4-amine (17). Pale-yellow solid (265 mg, 52%); mp 247–249 °C. ^{1}H NMR ([D$_6$]DMSO): δ 1.23 (d, J = 7.0 Hz, 3H, CH$_3$), 2.52–2.67, 2.74–2.81, 3.24–3.40 and 3.43–3.59 (4m, 8H, 2CH$_2$N morph + SCH$_2$CH$_2$), 3.65–3.80 (m, 4H, 2CH$_2$O morph), 3.85–3.90 (m, 1H, C̲H̲CH$_3$), 4.40–4.50 (m, 2H, CH$_2$N pyraz), 7.20–7.40 (m, 9H Ar), 7.97 (s, 1H, H-3), 10.40 (br s, 1H, NH disappears with D_2O). IR (cm^{-1}): 3450–3100 (NH). MS: m/z [M + 1]$^+$ 510. Anal. ($C_{26}H_{29}N_6OClS$) C, H, N, S.

1-(2-Chloro-2-phenylethyl)-6-(isopropylthio)-N-phenyl-1H-pyrazolo[3,4-d]pyrimidin-4-amine (21). Pale-yellow solid (263 mg, 62%); mp 152–153 °C. ^{1}H NMR (CDCl$_3$): δ 1.33 (d, J = 6.0 Hz, 3H, CH$_3$), 1.38 (d, J = 6.0 Hz, 3H, CH$_3$), 4.00 (sept, J = 6.0 Hz, 1H, SCH), 4.70–4.99 (m, 2H, CH$_2$N), 5.45–5.55 (m, 1H, CHCl), 7.00–7.51 (m, 11H, 10 Ar + H-3). IR (cm^{-1}): 3200–2800 (NH). MS: m/z [M + 1]$^+$ 425. Anal. ($C_{22}H_{22}N_5ClS$) C, H, N, S.

1-(2-Chloro-2-phenylethyl)-N-(3-fluorophenyl)-6-(isopropylthio)-1H-pyrazolo[3,4-d]pyrimidin-4-amine (22). White solid (208 mg, 47%); mp 217–218 °C. ^{1}H NMR (CDCl$_3$): δ 1.31 (d, J = 6.0 Hz, 3H, CH$_3$), 1.34 (d, J = 6.0 Hz, 3H, CH$_3$), 4.05 (sept, J = 6.0 Hz, 1H, SCH), 4.67–4.87 (m, 2H, CH$_2$N), 5.25–5.32 (m, 1H, CHCl), 6.88–7.51 (m, 10H, 9 Ar + H-3). IR (cm^{-1}): 3000–2500 (NH). MS: m/z [M + 1]$^+$ 443. Anal. ($C_{22}H_{21}N_5ClFS$) C, H, N, S.

N-(3-Bromophenyl)-1-(2-chloro-2-phenylethyl)-6-(isopropylthio)-1H-pyrazolo[3,4-d]pyrimidin-4-amine (23). Yellow solid (276 mg, 55%); mp 233–234 °C. ^{1}H NMR (CDCl$_3$): δ 1.28 (d, J = 6.0 Hz, 3H, CH$_3$), 1.31 (d, J = 6.0 Hz, 3H, CH$_3$), 4.10 (sept, J= 6.0 Hz, 1H, SCH), 4.78–4.91 (m, 2H, CH$_2$N), 5.35–5.47 (m, 1H, CHCl), 6.76–7.51 (m, 10H, 9 Ar + H-3). IR (cm^{-1}): 3000–2500 (NH). MS: m/z [M + 1]$^+$ 504. Anal. ($C_{22}H_{21}N_5BrClS$) C, H, N, S.

1-(2-Chloro-2-phenylethyl)-6-(cyclopentylthio)-N-phenyl-1H-pyrazolo[3,4-d]pyrimidin-4-amine (25). White solid (369 mg, 82%); mp 125–126 °C. ^{1}H NMR (CDCl$_3$): δ 1.52–1.78 (m, 8H, 4CH$_2$ cyclopent), 3.95–4.12 (m, 1H, SCH), 4.50–4.62 and 4.70–4.85 (2m, 2H, CH$_2$N), 5.22–5.40 (m, 1H, CHCl), 7.10–7.50 (m, 11H, 10 Ar + H-3). IR (cm^{-1}): 3363 (NH). MS: m/z [M + 1]$^+$ 451. Anal. ($C_{24}H_{24}N_5ClS$) C, H, N, S.

1-(2-Chloro-2-phenylethyl)-6-(cyclopentylthio)-N-(3-fluorophen-yl)-1H-pyrazolo[3,4-d]pyrimidin-4-amine (26). White solid (206 mg, 44%); mp 226–227 °C. ^{1}H NMR (CDCl$_3$): δ 1.78–1.84 and 2.12–2.43 (2m, 8H, 4CH$_2$ cyclopent), 3.98–4.17 (m, 1H, SCH), 4.54–4.68 and 4.73–4.89 (2m, 2H, CH$_2$N), 5.26–5.44 (m, 1H, CHCl), 5.54 (br s, 1H, NH disappears with D_2O), 6.93–7.53 (m, 10H, 9 Ar + H-3). IR (cm^{-1}): 2835 (NH). MS: m/z [M + 1]$^+$ 469. Anal. ($C_{24}H_{23}N_5ClFS$) C, H, N, S.

N-(3-Bromophenyl)-1-(2-chloro-2-phenylethyl)-6-[(2-morpholin-4-ylethyl)thio]-1H-pyrazolo[3,4-d]pyrimidin-4-amine (29). White solid (350 mg, 61%); mp 232–233 °C. ^{1}H NMR (CDCl$_3$): δ 2.90–3.99 (m, 12H, 4CH$_2$ morph + CH$_2$N + CH$_2$S), 4.63–4.85 and 5.04–5.21 (2m, 2H, CH$_2$N pyraz), 5.55–5.70 (m, 1H, CHCl), 7.03–8.52 (m, 10H, 9 Ar + H-3), 11.33 (br s, 1H, NH disappears with D_2O). IR (cm^{-1}): 3450 (NH). MS: m/z [M + 1]$^+$ 575. Anal. ($C_{25}H_{26}N_6OBrClS$) C, H, N, S.

General Procedure for the Synthesis of Compounds 10, 14, 18, 19, 20, 24, and 28. The 3-aminophenol (545 mg, 5 mmol) was added to a solution of the suitable 4-chloro derivative **32a–d** and **33a–d** (1 mmol) in absolute ethanol (10 mL), and the mixture was refluxed for 3–5 h. After cooling to room temperature, the solvent was evaporated under reduced pressure and the crude was solved in ethyl acetate (10 mL), washed with 0.1 N HCl solution (2 × 10 mL), 1 N NaOH solution (10 mL) and brine (2 × 10 mL), dried (MgSO$_4$), filtered, and concentrated under reduced pressure to give a brown oil which crystallized at 4 °C by adding a 1:1 mixture of diethyl ether/petroleum ether (bp 40–60 °C) (compounds **10**, **14**, **18**, **19**, **20**, and **24**) or cycloexane (**28**). If necessary, the solid obtained was purified by Silicagel chromatography column using CH$_2$Cl$_2$ as the eluent.

Compounds **10** and **18** were obtained as hydrochloride salts.

3-{[6-[(2-Morpholin-4-ylethyl)thio]-1-(2-phenylethyl)-1H-pyrazolo[3,4-d]pyrimidin-4-yl]amino}phenol Hydrochloride (10). Pale-yellow solid (261 mg, 51%); mp 261–262 °C. ^{1}H NMR (CDCl$_3$): δ 3.05–3.58 (m, 10H, CH$_2$Ar + 2CH$_2$N morph + SCH$_2$ + CH$_2$N), 3.77–3.95 (m, 4H, 2CH$_2$O morph), 4.57 (t, J = 7.0 Hz, 2H, CH$_2$N pyraz), 6.52–6.63 and 7.08–7.32 (2m, 10H, 9 Ar + H-3), 8.22 (br s, 1H, NH disappears with D_2O), 9.61 (br s, 1H disappears with D_2O), 10.18 (br s, 1H disappears with D_2O). IR (cm^{-1}): 3500–3100 (NH + OH). MS: m/z [M + 1]$^+$ 478. Anal. ($C_{25}H_{29}N_6O_2ClS$) C, H, N, S.

3-{[6-(Ethylthio)-1-(2-phenylpropyl)-1H-pyrazolo[3,4-d]-pyrimidin-4-yl]amino}phenol (14). Pale-yellow solid (296 mg, 73%); mp 184–186 °C. ^{1}H NMR (CDCl$_3$): δ 1.22 (d, J = 6.8 Hz, 3H, C̲H̲$_3$CH), 1.44 (t, J = 7.6 Hz, 3H, SCH$_2$C̲H̲$_3$), 3.19 (q, J = 7.6 Hz, 2H, SCH$_2$), 3.46–3.52 (m, 1H, C̲H̲CH$_3$), 4.36–4.89 (m, 2H, CH$_2$N), 6.82–6.84, 6.93–6.95, 6.99–7.05 and 7.16–7.24 (4m, 10H, 9 Ar + H-3). IR (cm^{-1}): 3200–2900 (NH + OH). MS: m/z [M + 1]$^+$ 407. Anal. ($C_{22}H_{23}N_5OS$) C, H, N, S.

3-{[6-[(2-Morpholin-4-ylethyl)thio]-1-(2-phenylpropyl)-1H-pyrazolo[3,4-d]pyrimidin-4-yl]amino}phenol Hydrochloride (18). Pale-yellow solid (248 mg, 47%); mp 177–178 °C. ^{1}H NMR (CDCl$_3$): δ 1.16–1.33 (m, 3H, CH$_3$), 2.60–2.80, 2.88–3.03 and 3.30–3.64 (3m, 9H, 2CH$_2$N morph + C̲H̲CH$_3$ + CH$_2$CH$_2$S), 3.78–3.97 (m, 4H, 2CH$_2$O morph), 4.38–4.55 (m, 2H, CH$_2$N pyraz), 6.54–6.74 and 7.09–7.33 (2m, 9H Ar), 7.58 (br s, 1H, disappears with D_2O), 7.92 (s, 1H, H-3), 8.18 (br s, 1H, disappears with D_2O). IR (cm^{-1}): 3500–3100 (NH + OH). MS: m/z [M + 1]$^+$ 492. Anal. ($C_{26}H_{31}N_6O_2ClS$) C, H, N, S.

3-{[1-(2-Chloro-2-phenylethyl)-6-(methylthio)-1H-pyrazolo[3,4-d]pyrimidin-4-yl]amino}phenol (19). Light-brown solid (132 mg, 32%); mp 82–83 °C. ^{1}H NMR (CDCl$_3$): δ 2.60 (s, 3H, CH$_3$), 4.72–4.77 and 4.84–4.90 (2m, 2H, CH$_2$N) 5.47–5.51 (m, 1H, CHCl), 6.78–6.80, 6.94–7.00 and 7.20–7.38 (3m, 11H, 9Ar + H-3 + 1H, 1H disappears with D_2O). IR (cm^{-1}): 3300–2910 (NH + OH). MS: m/z [M + 1]$^+$ 413. Anal. ($C_{20}H_{18}N_5OClS$) C, H, N, S.

3-{[6-(Butylthio)-1-(2-chloro-2-phenylethyl)-1H-pyrazolo[3,4-d]-pyrimidin-4-yl]amino}phenol (20). Light-brown solid (436 mg, 96%); mp 105–106 °C. ^{1}H NMR (CDCl$_3$): δ 0.99 (t, J = 7.2 Hz, 3H, CH$_3$), 1.52 (sx, J = 7.2 Hz, 2H, C̲H̲$_2$CH$_3$), 1.79 (quint, J = 7.2 Hz, 2H, C̲H̲$_2$CH$_2$CH$_3$), 3.14–3.24 (m, 2H, SCH$_2$), 4.68–4.73 and 4.83–4.89 (2m, 2H, CH$_2$N), 5.29 (br s, 1H, disappears with D_2O), 5.46–5.50 (m, 1H, CHCl), 6.78–6.80, 6.94–6.99 and 7.18–7.38 (3m, 11H, 9 Ar + H-3 + 1H, 1H disappears with D_2O). IR (cm^{-1}): 3400–3200 (NH + OH). MS: m/z [M + 1]$^+$ 455. Anal. ($C_{23}H_{24}N_5ClOS$) C, H, N, S.

3-{[1-(2-Chloro-2-phenylethyl)-6-(isopropylthio)-1H-pyrazolo-[3,4-d]pyrimidin-4-yl]amino}phenol (24). Light-brown solid (339 mg, 77%); mp 198–199 °C. ^{1}H NMR (CDCl$_3$): δ 1.46 (d, J = 6.0 Hz, 3H, CH$_3$), 1.49 (d, J = 6.0 Hz, 3H, CH$_3$), 3.97–4.07 (m, 1H, SCH), 4.70–4.75 and 4.83–4.88 (2m, 2H, CH$_2$N) 5.48–5.51 (m, 1H, CHCl), 6.78–6.80, 6.94–7.02 and 7.21–7.41 (3m, 10H, 9 Ar + H-3). IR (cm^{-1}): 3300–3100 (NH + OH). MS: m/z [M + 1]$^+$ 441. Anal. ($C_{22}H_{22}N_5ClOS$) C, H, N, S

3-{[1-(2-Chloro-2-phenylethyl)-6-(cyclopentylthio)-1H-pyrazolo-[3,4-d]pyrimidin-4-yl]amino}phenol (28). White solid (359 mg, 77%); mp 160–161 °C. ^{1}H NMR (CDCl$_3$): δ 1.62–2.24 (m, 8H, 4CH$_2$ cyclopent), 4.03–4.22 (m, 1H, SCH), 4.75–4.95 (m, 2H, CH$_2$N), 5.45–5.56 (m, 1H, CHCl), 6.80–7.60 (m, 9H Ar), 8.06 (s, 1H H-3), 10.20 (br s, 1H, disappears with D_2O). IR (cm^{-1}): 3500–3000 (NH + OH). MS: m/z [M + 1]$^+$ 467. Anal. ($C_{24}H_{24}N_5OClS$) C, H, N, S.

ADME Assays. *Chemicals.* All solvents and reagents were from Sigma-Aldrich Srl (Milan, Italy), and Brain Polar Lipid Extract (Porcine) was from Avanti Polar Lipids, Inc. (Alabama, USA). Dodecane was purchased from Fluka (Milan, Italy). Pooled male donors 20 mg mL^{-1} HLM were from BD Gentest-Biosciences (San Jose, California). Milli-Q quality water (Millipore, Milford, MA, USA) was used. Hydrophobic filter plates (MultiScreen-IP, clear plates, 0.45 μm diameter pore size), 96-well microplates, and 96-well UV-transparent microplates were obtained from Millipore (Bedford, MA, USA).

Parallel Artificial Membrane Permeability Assay (PAMPA). Donor solution (0.5 mM) was prepared by diluting 1 mM dimethyl sulfoxide (DMSO) compound stock solution using phosphate buffer (pH 7.4, 0.025 M). Filters were coated with 5 μL of a 1% (w/v) dodecane solution of phosphatidylcholine or 4 μL of brain polar lipid solution (20 mg mL^{-1} 16% CHCl$_3$, 84% dodecane), prepared from CHCl$_3$ solution 10% w/v, for intestinal permeability and BBB permeability, respectively. Donor solution (150 μL) was added to each well of the filter plate. To each well of the acceptor plate were added 300 μL of solution (50% DMSO in phosphate buffer). All compounds were tested in three different plates on different days. The sandwich was incubated for 5 h at room temperature under gentle shaking. After the incubation time, the plates were separated and samples were taken from both receiver and donor sides and analyzed using LC with UV detection at 280 nm.

LC analysis were performed with a Varian Prostar HPLC system (Varian Analytical Instruments, USA) equipped with a binary pump with a manual injection valve and model Prostar 325 UV−vis detector. Chromatographic separation were conducted using a Polaris C18-A column (150−4.6 mm, 5 μm particle size) at a flow rate of 0.8 mL min^{-1} with a mobile phase composed of 60% ACN/40% H$_2$O−formic acid 0.1%.

Permeability (P_{app}) for PAMPA was calculated according to the following equation, obtained from Wohnsland and Faller[51] and Sugano et al.[52] equation with some modification in order to obtain permeability values in cm s^{-1},

$$P_{app} = \frac{V_D V_A}{(V_D + V_A)At} - \ln(1 - r)$$

where V_A is the volume in the acceptor well, V_D is the volume in the donor well (cm^3), A is the "effective area" of the membrane (cm^2), t is the incubation time (s), and r the ratio between drug concentration in the acceptor and equilibrium concentration of the drug in the total volume ($V_D + V_A$). Drug concentration was estimated by using the peak area integration.

Membrane retentions (%) were calculated according to the following equation:

$$\%MR = \frac{[r - (D + A)] \times 100}{Eq}$$

where r is the ratio between drug concentration in the acceptor and equilibrium concentration, D, A, and Eq represented drug concentration in the donor, acceptor, and equilibrium solution, respectively.

Water Solubility Assay. Each solid compound (1 mg) was added to 1 mL of water. The samples were shaked in a shaker bath at room temperature for 24−36 h. The suspensions were filtered through a 0.45 μm nylon filter (Acrodisc), and the solubilized compound determined by LC−MS−MS assay. For each compound, the determination was performed in triplicate.

For the quantification was used an LC−MS system consisted of a Varian apparatus (Varian Inc.) including a vacuum solvent degassing unit, two pumps (212-LC), a triple quadrupole MSD (model 320-LC) mass spectrometer with ES interface, and Varian MS Workstation System Control version 6.9 software. Chromatographic separation was obtained using a Pursuit C18 column (50 mm × 2.0 mm) (Varian) with 3 μm particle size and gradient elution: eluent A being ACN and eluent B consisting of an aqueous solution of formic acid (0.1%). The analysis started with 0% of eluent A, which was linearly increased up to 70% in 10 min, then slowly increased up to 98% up to 15 min. The flow rate was 0.2 mL min^{-1}, and injection volume was 5 μL. The instrument operated in positive mode and parameters were: detector 1850 V, drying gas pressure 25.0 psi, desolvation temperature 300.0 °C, nebulizing gas 40.0 psi, needle 5000 V, and shield 600 V. Nitrogen was used as nebulizer gas and drying gas. Collision induced dissociation was performed using argon as the collision gas at a pressure of 1.8 mTorr in the collision cell. The transitions as well as the capillary voltage and the collision energy used for each compound are summarized in Supporting Information, Table S3.

Quantification of the single compound was made by comparison with apposite calibration curves realized with standard solutions in methanol.

Microsomal Stability Assay. Each compound in DMSO solution was incubated at 37 °C for 60 min in 125 mM phosphate buffer (pH 7.4) and 5 μL of human liver microsomal protein (0.2 mg mL^{-1}), in the presence of a NADPH-generating system at a final volume of 0.5 mL (compound final concentration, 50 μM); DMSO did not exceed 2% (final solution). The reaction was stopped by cooling on ice and adding 1.0 mL of acetonitrile. The reaction mixtures were then centrifuged, and the parent drug and metabolites were subsequently determined by LC−UV−MS.

Chromatographic analysis was performed with an Agilent 1100 LC/MSD VL system (G1946C) (Agilent Technologies, Palo Alto, CA) constituted by a vacuum solvent degassing unit, a binary high-pressure gradient pump, an 1100 series UV detector, and an 1100 MSD model VL benchtop mass spectrometer.

Chromatographic separation was obtained using a Varian Polaris C18-A column (150−4.6 mm, 5 μm particle size) and gradient elution: eluent A being ACN and eluent B consisting of an aqueous solution of formic acid (0.1%). The analysis started with 2% of eluent A, which was rapidly increased up to 70% in 12 min, then slowly increased up to 98% in 20 min. The flow rate was 0.8 mL min^{-1} and injection volume was 20 μL.

The Agilent 1100 series mass spectra detection (MSD) single-quadrupole instrument was equipped with the orthogonal spray API-ES (Agilent Technologies, Palo Alto, CA). Nitrogen was used as nebulizing and drying gas. The pressure of the nebulizing gas, the flow of the drying gas, the capillary voltage, the fragmentor voltage, and the vaporization temperature were set at 40 psi, 9 L/min, 3000 V, 70 V, and 350 °C, respectively. UV detection was monitored at 280 nm. The LC−ESI−MS determination was performed by operating the MSD in the positive ion mode. Spectra were acquired over the scan range m/z 100−1500 using a step size of 0.1 μ. The percentage of not metabolized compound was calculated by comparison with reference solutions.

Biological Studies. *Enzymatic Assay on Isolated Src.* Recombinant human Src was purchased from Upstate (Lake Placid, NY). Activity was measured in a filter-binding assay using a commercial kit (Src Assay Kit, Upstate), according to the manufacturer's protocol, using 150 μM of the specific Src peptide substrate (KVEKIGEG-TYGVVYK) and in the presence of 0.125 pMol of Src and 10 μM of [γ-^{32}P]-ATP. The apparent affinity (K_m) values of the Src preparation used for its peptide and ATP substrates were determined separately and found to be 30 μM and 5 μM, respectively.

Enzymatic Assay on Isolated Abl. Recombinant human Abl was purchased from Upstate. Activity was measured in a filter binding assay using an Abl specific peptide substrate (Abtide, Upstate). Reaction conditions were: 10 μM [γ-^{32}P]-ATP, 50 μM peptide, 0.022 μM c-Abl. The apparent affinity (K_m) values of the Abl preparation used for its peptide and ATP substrates were determined separately and found to be 1.5 and 10 μM, respectively.

Cell Cycle and Apoptosis Analysis. Cells were seeded in 60 mm Petri dishes at a density of 3 × 10^5. After treatment and subsequent incubation for 24 h at 37 °C and 5% CO$_2$ in humidified atmosphere, harvested cells were washed and fixed overnight with 70% ethanol. Then ethanol was removed by centrifugation and the cells resuspended in PBS and stained with 50 μg/mL propidium iodide (PI) at 4 °C for 30 min in the dark. Stained cells were analyzed by Tali image based cytometer (Life Technologies, Carlsbad, CA, USA) counting 20 fields for sample and exported fcs raw. Apoptosis led to the fragmentation of DNA and formation of apoptotic bodies with a progressive loss of DNA content from cells in the G1 phase. For this reason, the fluorescence signals lower but adjacent to the G1 phase signals (hypodiploid peak) are considered an effective estimation for apoptotic cells (percentage respect to total events). Data were elaborated by Flowing software (v. 2.5.0, by Perttu Terho, University of Turku, Finland).

Spheroid Growth Assay. The in vitro antitumoral action of inhibitors was evaluated by neuroblastoma spheroid assay. The SH-

SY5Y cell line was utilized as cell model of human neuroblastoma. Cells were purchased from American Type Culture Collection (ATCC, Manassas, VA, USA) and were cultured in DMEM medium supplemented with 10% fetal bovine serum. IBIDI angiogenesis microslides (IBIDI GmbH) were coated with growth factor reduced Matrigel (BD, Bioscience) and allowed to polymerize for 30 min. SH-SY5Y cells were seeded in a 96-multiwell plate in the presence or not (CTR) of inhibitors. Starting from 24 h after the seeding, in basal condition, cellular aggregates with spheroidal appearance (diameter >100 μm) were visible. The size of cellular spheres, in terms of area and diameter, was determined using an Image Pro-plus v 4.5 analysis system considering five random fields/treatment ($400\times$ magnification). IC_{50} (drug concentration that determined the 50% of growth inhibition) was calculated by Grafit v4.0 (Erithacus Software Limited) software using the best fitting sigmoid curve. For cytotoxicity studies, the Wi38 human diploid cell line was derived from normal embryonic lung tissue and was purchased from ATCC.

Animals and Experimental in Vivo Model. Male CD1 nude mice (Charles River, Milan, Italy) were maintained under the guidelines established by our Institution (University of L'Aquila, Medical School and Science and Technology School Board Regulations, complying with the Italian government regulation no. 116, January 27, 1992, for the use of laboratory animals). Before any invasive manipulation, mice were anesthetized with a mixture of ketamine (25 mg/mL)/xylazine (5 mg/mL). Tumor grafts were obtained by injecting sc 1×10^6 SH-SY5Y cells in 100 μL of 12 mg/mL Matrigel (Becton Dickinson, Franklin Lakes, NJ, USA). Tumor growth was monitored daily by measuring the average tumor diameter. The tumor volume was expressed in mm^3 according to the formula $4/3\pi r^3$. For in vivo administration, **29** was prepared as suspension in 0.5% methylcellulose solution. Each mouse received daily oral administration of methylcellulose vehicle or of 50 mg/kg **29**.

Cytofluorimetric Analysis. Analysis of DNA content was performed for the evaluation of the cell cycle; 0.5×10^6 SH-SY5Y cells were plated in 100 mm dishes and treated the next day with **29** for 72 h. Then cells were detached with trypsin, fixed in cold 70% ethanol at 4 °C for 2 h, resuspended in 500 μL of staining solution (40 μg/mL propidium iodide and 500 μg/mL RNase A in PBS; all from Sigma) for 30 min at 37 °C, and analyzed by flow cytometry. A FACSCalibur (BD Biosciences) flow cytometer was used, and the analysis was performed with FlowJo software (BD Biosciences).

Sprouting Assay. The brain microvascular endothelial cell line hBMEC was purchased from ScienCell Research Laboratory (Carlsbad, CA, USA). HBMEC cells were suspended in culture medium containing 20% methylcellulose, seeded at a density of 1000 cells/well, into nonadhesive 96-well plate and cultured at 37 °C (5% CO$_2$, 100% humidity). Under these conditions, suspended endothelial cells (EC) form spontaneously within 4 h a single cell aggregate known as a spheroid. Spheroids were harvested within 24 h and used for in-gel sprouting angiogenesis experiments. Briefly, spheroids were seeded in microslides coated with Matrigel and images were observed after 24 h, captured by an inverted microscope and analyzed with the NIH ImageJ analysis system. For statistical analysis, number of sprouts per spheroid, with a minimum of 10 spheroids for each treatment, was considered.

ASSOCIATED CONTENT

Ⓢ Supporting Information

Experimental details of enantiomers separation, a figure for the evaluation of compound **29** toward SH-SY5Y cell growth, data collection and refinement statistics of the X-ray complex, elemental analysis for new synthesized compounds, chromatographic and MS parameters. This material is available free of charge via the Internet at http://pubs.acs.org.

AUTHOR INFORMATION

Corresponding Author

*Phone: (+39) 010 353 8362. E-mail: schensil@unige.it.

Present Address

◆For M.R.: Dipartimento di Farmacia, University of Parma, Parco Area delle Scienze 27/A, Parma 43124, Italy.

Notes

The authors declare no competing financial interest.

REFERENCES

(1) *Surveillance, Epidemiology and End Results Database*; National Cancer Institute: Bethesda, MD; http://seer.cancer.gov (accessed November 2005).

(2) Brodeur, G. M.; Maris, J. M. Neuroblastoma. In *Principles and Practice of Pediatric Oncology*, 5th ed.; Pizzo, P. A., Poplack, D. G., Eds.; J B Lippincott Company: Philadelphia, 2006; pp 933−970.

(3) De Bernardi, B.; Nicolas, B.; Boni, L.; Indolfi, P.; Carli, M.; Cordero Di Montezemolo, L.; Donfrancesco, A.; Pession, A.; Provenzi, M.; di Cataldo, A.; Rizzo, A.; Tonini, G. P.; Dallorso, S.; Conte, M.; Gambini, C.; Garaventa, A.; Bonetti, F.; Zanazzo, A.; D'Angelo, P.; Bruzzi, P. Disseminated neuroblastoma in children older than one year at diagnosis: comparable results with three consecutive high-dose protocols adopted by the Italian Co-Operative Group for Neuroblastoma. *J. Clin. Oncol.* **2003**, *21*, 1592−601.

(4) Matthay, K. K.; Villablanca, J. G.; Seeger, R. C.; Stram, D. O.; Harris, R. E.; Ramsay, N. K.; Swift, P.; Shimada, H.; Black, C. T.; Brodeur, G. M.; Gerbing, R. B.; Reynolds, C. P. Treatment of high-risk neuroblastoma with intensive chemotherapy, radiotherapy, autologous bone marrow transplantation, and 13-*cis*-retinoic acid. Children's Cancer Group. *N. Engl. J. Med.* **1999**, *341*, 1165−1173.

(5) Brodeur, G. M. Neuroblastoma: biological insights into a clinical enigma. *Nature Rev. Cancer* **2003**, *3*, 203−216.

(6) Maris, J. M.; Hogarty, M. D.; Bagatell, R.; Cohn, S. L. Neuroblastoma. *Lancet* **2007**, *369*, 2106−2120.

(7) Arora, A.; Scholar, E. M. Role of tyrosine kinase inhibitors in cancer therapy. *J. Pharmacol. Exp. Ther.* **2005**, *315*, 971−979.

(8) Pytel, D.; Sliwinski, T.; Poplawski, T.; Ferriola, D.; Majsterek, I. Tyrosine kinase blockers: new hope for successful cancer therapy. *Anticancer Agents Med. Chem.* **2009**, *9*, 66−76.

(9) (a) Brunton, V. G.; Frame, M. C. Src and focal adhesion kinase as therapeutic targets in cancer. *Curr. Opin. Pharmacol.* **2008**, *8*, 427−432. (b) Schenone, S.; Manetti, F.; Botta, M. SRC inhibitors and angiogenesis. *Curr. Pharm. Des.* **2007**, *13*, 2118−2128.

(10) Grant, S.; Dent, P. Kinase inhibitors and cytotoxic drug resistance. *Clin. Cancer Res.* **2004**, *10*, 2205−2207.

(11) Huang, H.; Ma, J.; Shi, J.; Meng, L.; Jiang, H.; Ding, J.; Liu, H. Discovery of novel purine derivatives with potent and selective inhibitory activity against c-Src tyrosine kinase. *Bioorg. Med. Chem.* **2010**, *18*, 4615−4624.

(12) Wang, Y.; Shakespeare, W. C.; Huang, W. S.; Sundaramoorthi, R.; Lentini, S.; Das, S.; Liu, S.; Banda, G.; Wen, D.; Zhu, X.; Xu, Q.; Keats, J.; Wang, F.; Wardwell, S.; Ning, Y.; Snodgrass, J. T.; Broudy, M. I.; Russian, K.; Dalgarno, D.; Clackson, T.; Sawyer, T. K. Novel N9-arenethenyl purines as potent dual Src/Abl tyrosine kinase inhibitors. *Bioorg. Med. Chem. Lett.* **2008**, *18*, 4907−4912.

(13) Hennequin, L. F.; Allen, J.; Breed, J.; Curwen, J.; Fennell, M.; Green, T. P.; Lambert-van der Brempt, C.; Morgentin, R.; Norman, R. A.; Olivier, A.; Otterbein, L.; Plé, P. A.; Warin, N.; Costello, G. N-(5-Chloro-1,3-benzodioxol-4-yl)-7-[2-(4-methylpiperazin-1-yl)ethoxy]-5-

(tetrahydro-2*H*-pyran-4-yloxy)quinazolin-4-amine, a novel, highly selective, orally available, dual-specific c-Src/Abl kinase inhibitor. *J. Med. Chem.* **2006**, *49*, 6465−6488.

(14) Cao, X.; You, Q. D.; Li, Z. Y.; Guo, Q. L.; Shang, J.; Yan, M.; Chern, J. W.; Chen, M. L. Design and synthesis of 7-alkoxy-4-heteroarylamino-3-quinolinecarbonitriles as dual inhibitors of c-Src kinase and nitric oxide synthase. *Bioorg. Med. Chem.* **2008**, *16*, 5890−5898.

(15) Palanki, M. S.; Cao, J.; Chow, C. P.; Dneprovskaia, E.; Mak, C. C.; McPherson, A.; Pathak, V. P.; Renick, J.; Soll, R.; Zeng, B.; Noronha, G. Development of novel benzotriazines for drug discovery. *Expert Opin. Drug Discovery* **2009**, *4*, 33−49.

(16) Das, J.; Chen, P.; Norris, D.; Padmanabha, R.; Lin, J.; Moquin, R. V.; Shen, Z.; Cook, L. S.; Doweyko, A. M.; Pitt, S.; Pang, S.; Shen, D. R.; Fang, Q.; de Fex, H. F.; McIntyre, K. W.; Shuster, D. J.; Gillooly, K. M.; Behnia, K.; Schieven, G. L.; Wityak, J.; Barrish, J. C. 2-Aminothiazole as a novel kinase inhibitor template. Structure−activity relationship studies toward the discovery of *N*-(2-chloro-6-methylphenyl)-2-[[6-[4-(2-hydroxyethyl)-1-piperazinyl)]-2-methyl-4-pyrimidinyl]amino)]-1,3 thiazole-5-carboxamide (dasatinib, BMS-354825) as a potent pan-Src kinase inhibitor. *J. Med. Chem.* **2006**, *49*, 6819−6832.

(17) Schenone, S.; Brullo, C.; Musumeci, F.; Botta, M. Novel dual Src/Abl inhibitors for hematologic and solid malignancies. *Expert Opin. Invest. Drugs* **2010**, *19*, 931−945.

(18) (a) Bolen, J. B.; Rosen, N.; Israel, M. A. Increased pp60c-src tyrosyl kinase activity in human neuroblastoma is associated with amino-terminal tyrosine phosphorylation of the src gene product. *Proc. Natl. Acad. Sci. U. S. A.* **1985**, *82*, 7275−7279. (b) O'Shaughnessy, J.; Deseau, V.; Amini, S.; Rosen, N.; Bolen, J. B. Analysis of the c-src gene product structure, abundance, and protein kinase activity in human neuroblastoma and glioblastoma cells. *Oncogene Res.* **1987**, *2*, 1−18. (c) Bjelfman, C.; Hedborg, F.; Johansson, I.; Nordenskjold, M.; Pahlman, S. Expression of the neuronal form of pp60c-src in neuroblastoma in relation to clinical stage and prognosis. *Cancer Res.* **1990**, *50*, 6908−6914. (d) Matsunaga, T.; Takahashi, H.; Ohnuma, N.; Tanabe, M.; Yoshida, H.; Iwai, J.; Shirasawa, H.; Simizu, B. Expression of *N*-myc and c-src proto-oncogenes correlating to the undifferentiated phenotype and prognosis of primary neuroblastomas. *Cancer Res.* **1991**, *51*, 3148−3152. (e) Finlay, D.; Vuori, K. Novel noncatalytic role for caspase-8 in promoting SRC-mediated adhesion and Erk signaling in neuroblastoma cells. *Cancer Res.* **2007**, *67*, 11704−11711.

(19) (a) Matsunaga, T.; Shirasawa, H.; Tanabe, M.; Ohnuma, N.; Takahashi, H.; Simizu, B. Expression of alternatively spliced src messenger RNAs related to neuronal differentiation in human neuroblastomas. *Cancer Res.* **1993**, *53*, 3179−3185. (b) Matsunaga, T.; Shirasawa, H.; Tanabe, M.; Ohnuma, N.; Kawamura, K.; Etoh, T.; Takahashi, H.; Simizu, B. Expression of neuronal Src mRNA as a favorable marker and inverse correlation to *N*-myc gene amplification in human neuroblastomas. *Int. J. Cancer* **1994**, *58*, 793−798.

(20) Hishiki, T.; Saito, T.; Sato, Y.; Mitsunaga, T.; Terui, E.; Matsuura, G.; Saito, E.; Shibata, R.; Mise, N.; Yokoyama, Y.; Yoshida, H. Src kinase familyinhibitor PP2 induces aggregation and detachment of neuroblastoma cells and inhibits cell growth in a PI3 kinase/Akt pathway-independent manner. *Pediatr. Surg. Int.* **2011**, *27*, 225−230.

(21) Vitali, R.; Mancini, C.; Cesi, V.; Tanno, B.; Piscitelli, M.; Mancuso, M.; Sesti, F.; Pasquali, E.; Calabretta, B.; Dominici, C.; Raschellà, G. Activity of tyrosine kinase inhibitor Dasatinib in neuroblastoma cells in vitro and in orthotopic mouse model. *Int. J. Cancer* **2009**, *125*, 2547−2555.

(22) (a) Carraro, F.; Pucci, A.; Naldini, A.; Schenone, S.; Bruno, O.; Ranise, A.; Bondavalli, F.; Brullo, C.; Fossa, P.; Menozzi, G.; Mosti, L.; Manetti, F.; Botta, M. Pyrazolo[3,4-*d*]pyrimidines endowed with antiproliferative activity on ductal infiltrating carcinoma cells. *J. Med. Chem.* **2004**, *47*, 1595−1598. (b) Carraro, F.; Naldini, A.; Pucci, A.; Locatelli, G. A.; Maga, G.; Schenone, S.; Bruno, O.; Ranise, A.; Bondavalli, F.; Brullo, C.; Fossa, P.; Menozzi, G.; Mosti, L.; Modugno, M.; Tintori, C.; Manetti, F.; Botta, M. Pyrazolo[3,4-*d*]pyrimidines as potent antiproliferative and proapoptotic agents toward A431 and

8701-BC cells in culture via inhibition of c-Src phosphorylation. *J. Med. Chem.* **2006**, *49*, 1549−1561. (c) Manetti, F.; Santucci, A.; Locatelli, G. A.; Maga, G.; Spreafico, A.; Serchi, T.; Orlandini, M.; Bernardini, G.; Caradonna, N. P.; Spallarossa, A.; Brullo, C.; Schenone, S.; Bruno, O.; Ranise, A.; Bondavalli, F.; Hoffmann, O.; Bologna, M.; Angelucci, A.; Botta, M. Identification of a novel pyrazolo[3,4-*d*]pyrimidine able to inhibit cell proliferation of a human osteogenic sarcoma in vitro and in a xenograft model in mice. *J. Med. Chem.* **2007**, *50*, 5579−5588. (d) Angelucci, A.; Schenone, S.; Gravina, G. L.; Muzi, P.; Festuccia, C.; Vicentini, C.; Botta, M.; Bologna, M. Pyrazolo[3,4-*d*]pyrimidines c-Src inhibitors reduce epidermal growth factor-induced migration in prostate cancer cells. *Eur. J. Cancer* **2006**, *42*, 2838−2845.

(23) Navarra, M.; Celano, M.; Maiuolo, J.; Schenone, S.; Botta, M.; Angelucci, A.; Bramanti, P.; Russo, D. Antiproliferative and pro-apoptotic affects afforded by nove Src-kinase inhibitors in human neuroblastoma cells. *BMC Cancer* **2010**, *10*, 602.

(24) Delle Monache, S.; Sanità, P.; Calgani, A.; Schenone, S.; Botta, L.; Angelucci, A. Src inhibition potentiates antitumoral effect of paclitaxel by blocking tumor-induced angiogenesis. *Exp. Cell Res.* **2014**, *328*, 20−31.

(25) Radi, M.; Brullo, C.; Crespan, E.; Tintori, C.; Musumeci, F.; Biava, M.; Schenone, S.; Dreassi, E.; Zamperini, C.; Maga, G.; Pagano, D.; Angelucci, A.; Bologna, M.; Botta, M. Identification of potent c-Src inhibitors strongly affecting the proliferation of human neuroblastoma cells. *Biomed. Chem. Lett.* **2011**, *21*, 5928−5933.

(26) Radi, M.; Dreassi, E.; Brullo, C.; Crespan, E.; Tintori, C.; Bernardo, V.; Valoti, M.; Zamperini, C.; Daigl, H.; Musumeci, F.; Carraro, F.; Naldini, A.; Filippi, I.; Maga, G.; Schenone, S.; Botta, M. Design, synthesis, biological activity, and ADME properties of pyrazolo[3,4-*d*]pyrimidines active in hypoxic human leukemia cells: a lead optimization study. *J. Med. Chem.* **2011**, *54*, 2610−2626.

(27) Xu, W.; Doshi, A.; Lei, M.; Eck, M. J.; Harrison, S. C. Crystal structures of c-Src reveal features of its autoinhibitory mechanism. *Cell* **1999**, *3*, 629−638.

(28) Cowan-Jacob, S. W.; Fendrich, G.; Manley, P. W.; Jahnke, W.; Fabbro, D.; Liebetanz, J.; Meyer, T. The crystal structure of a c-Src complex in an active conformation suggests possible steps in c-Src activation. *Structure* **2005**, *13*, 861−871.

(29) (a) Simard, J. R.; Klüter, S.; Grütter, C.; Getlik, M.; Rabiller, M.; Rode, H. B.; Rauh, D. A new screening assay for allosteric inhibitors of cSrc. *Nature Chem. Biol.* **2009**, *5*, 394−396. (b) Getlik, M.; Grütter, C.; Simard, J. R.; Klüter, S.; Rabiller, M.; Rode, H. B.; Robubi, A.; Rauh, D. Hybrid compound design to overcome the gatekeeper T338M mutation in cSrc. *J. Med. Chem.* **2009**, *52*, 3915−3926.

(30) Jorgensen, W. L.; Thomas, L. T. Perspective on free-energy perturbation calculations for chemical equilibria. *J. Chem. Theory Comput.* **2008**, *4*, 869−876.

(31) Jorgensen, W. L.; Schyman, P. Treatment of Halogen Bonding in the OPLS-AA Force Field; Application to Potent Anti-HIV Agents. *J. Chem. Theory Comput.* **2012**, *8*, 3895−3801.

(32) (a) Falchi, F.; Manetti, F.; Carraro, F.; Naldini, A.; Maga, G.; Crespan, E.; Schenone, S.; Bruno, O.; Brullo, C.; Botta, M. 3D-QSAR models built on structure-based alignments of Abl tyrosine kinase inhibitors. *ChemMedChem* **2009**, *4*, 976−987. (b) Alcaro, S.; Artese, A.; Botta, M.; Zizzarri, A.; Orallo, F.; Ortuso, F.; Schenone, S.; Brullo, C.; Yáñez, M. Hit identification and biological evaluation of anticancer pyrazolopyrimidines endowed with anti-inflammatory activity. *ChemMedChem* **2010**, *5*, 1242−1246.

(33) Kruewel, T.; Schenone, S.; Radi, M.; Maga, G.; Rohrbeck, A.; Botta, M.; Borlak, J. Molecular characterization of c-Abl/c-Src kinase inhibitors targeted against murine tumour progenitor cells that express stem cell markers. *PloS One* **2010**, *5*, e14143.

(34) Vignaroli, G.; Mencarelli, M.; Sementa, D.; Crespan, E.; Kissova, M.; Maga, G.; Schenone, S.; Radi, M.; Botta, M. Exploring the chemical space around the privileged pyrazolo[3,4-*d*]pyrimidine scaffold: toward novel allosteric inhibitors of T315I-mutated Abl. *ACS Comb. Sci.* **2014**, *16*, 168−175.

(35) Dalgarno, D.; Stehle, T.; Narula, S.; Schelling, P.; van Schravendijk, M. R.; Adams, S.; Andrade, L.; Keats, J.; Ram, M.; Jin,

L.; Grossman, T.; MacNeil, I.; Metcalf, C., III; Shakespeare, W.; Wang, Y.; Keenan, T.; Sundaramoorthi, R.; Bohacek, R.; Weigele, M.; Sawyer, T. Structural basis of Src tyrosine kinase inhibition with a new class of potent and selective trisubstituted purine-based compounds. *Chem. Biol. Drug Des.* **2006**, *67*, 46−57.

(36) Michalczyk, A.; Klüter, S.; Rode, H. B.; Simard, J. R.; Grütter, C.; Rabiller, M.; Rauh, D. Structural insights into how irreversible inhibitors can overcome drug resistance in EGFR. *Bioorg. Med. Chem.* **2008**, *16*, 3482−3488.

(37) Kabsch, W. Automatic processing of rotation diffraction data from crystals of initially unknown symmetry and cell constants. *J. Appl. Crystallogr.* **1993**, *26*, 795−800.

(38) Zeng, X.; Gipson, B.; Zheng, Z. Y.; Renault, L.; Stahlberg, H. Automatic lattice determination for two-dimensional crystal images. *J. Struct. Biol.* **2007**, *160*, 353−361.

(39) Read, R. J. Pushing the boundaries of molecular replacement with maximum likelihood. *Acta Crystallogr., Sect. D: Biol. Crystallogr.* **2001**, *57*, 1373−1382.

(40) Seeliger, M. A.; Nagar, B.; Frank, F.; Cao, X.; Henderson, M. N.; Kuriyan, J. c-Src binds to the cancer drug imatinib with an inactive Abl/c-Kit conformation and a distributed thermodynamic penalty. *Structure* **2007**, *15*, 299−311.

(41) Emsley, P.; Cowtan, K. Coot: model-building tools for molecular graphics. *Acta Crystallogr., Sect. D: Biol. Crystallogr.* **2004**, *60*, 2126−2132.

(42) Brünger, A. T.; Adams, P. D.; Clore, G. M.; DeLano, W. L.; Gros, P.; Grosse-Kunstleve, R. W.; Jiang, J. S.; Kuszewski, J.; Nilges, M.; Pannu, N. S.; Read, R. J.; Rice, L. M.; Simonson, T.; Warren, G. L. Crystallography & NMR system: A new software suite for macromolecular structure determination. *Acta Crystallogr., Sect. D: Biol. Crystallogr.* **1998**, *54*, 905−921.

(43) Murshudov, G. N.; Vagin, A. A.; Dodson, E. J. Refinement of macromolecular structures by the maximum-likelihood method. *Acta Crystallogr., Sect. D: Biol. Crystallogr.* **1997**, *53*, 240−255.

(44) Schüttelkopf, A. W.; van Aalten, D. M. PRODRG: a tool for high-throughput crystallography of protein−ligand complexes. *Acta Crystallogr., Sect. D: Biol. Crystallogr.* **2004**, *60*, 1355−1363.

(45) Laskowski, R. A.; MacArthur, M. W.; Moss, D. S.; Thornton, J. M. PROCHECK: a program to check the stereochemical quality of protein structures. *J. Appl. Crystallogr.* **1993**, *26*, 283−291.

(46) *Prime*, v3.1; Schrodinger, LLC: New York, 2012.

(47) Jacobson, M. P.; Pincus, D. L.; Rapp, C. S.; Day, T. J. F.; Honig, B.; Shaw, D. E.; Friesner, R. A. A. Hierarchical approach to all-atom protein loop prediction. *Proteins: Struct., Funct., Bioinf.* **2004**, *55*, 351−367.

(48) Zeevaart, J. G.; Wang, L.; Thakur, V. V.; Leung, C. S.; Tirado-Rives, J.; Bailey, C. M.; Domaoal, R. A.; Anderson, K. S.; Jorgensen, W. L. Optimization of azoles as anti-HIV agents guided by free-energy calculations. *J. Am. Chem. Soc.* **2008**, *130*, 9492−9499.

(49) Leung, C. S.; Zeevaart, J. G.; Domaoal, R. A.; Bollini, M.; Thakur, V. V.; Spasov, K.; Anderson, K. S.; Jorgensen, W. L. Eastern extension of azoles as non-nucleoside inhibitors of HIV-1 reverse transcriptase; cyano group alternatives. *Bioorg. Med. Chem. Lett.* **2010**, *20*, 2485−2488.

(50) Jorgensen, W. L.; Tirado-Rives, J. Molecular modeling of organic and biomolecular systems using BOSS and MCPRO. *J. Comput. Chem.* **2005**, *26*, 1689−1700.

(51) Wohnsland, F.; Faller, B. High-throughput permeability pH profile and high-throughput alkane/water log P with artificial membranes. *J. Med. Chem.* **2001**, *44*, 923−930.

(52) Sugano, K.; Hamada, H.; Machida, M.; Ushio, H. High throughput prediction of oral absorption: improvement of the composition of the lipid solution used in parallel artificial membrane permeation assay. *J. Biomol. Screening* **2001**, *6*, 189−196.